Bioorganic Chemistry 86 (2019) 80–96

Contents lists available at ScienceDirect

Bioorganic Chemistry

journal homepage: www.elsevier.com/locate/bioorg

New thiazol-hydrazono-coumarin hybrids targeting human cervical cancer cells: Synthesis, CDK2 inhibition, QSAR and molecular docking studies

Somaia S. Abd El-Karim[a], Yasmin M. Syam[a,*], Ahmed M. El Kerdawy[b,c,d], Tamer M. Abdelghany[e]

[a] Therapeutical Chemistry Department, National Research Centre, Dokki, Cairo, P. O. Box 12622, Egypt
[b] Department of Pharmaceutical Chemistry, Faculty of Pharmacy, Cairo University, Kasr El-Aini Street, Cairo, P.O. Box 11562, Egypt
[c] Molecular Modeling Unit, Faculty of Pharmacy, Cairo University, Kasr El-Aini Street, Cairo, P.O. Box 11562, Egypt
[d] Department of Pharmaceutical Chemistry, Faculty of Pharmacy, New Giza University, Newgiza, km 22 Cairo–Alexandria Desert Road, Cairo, Egypt
[e] Department of Pharmacology, Faculty of Pharmacy, Al-Azhar University, Nasr City, Cairo, P.O. Box 11787, Egypt

ARTICLE INFO

Keywords:
2-Aminothiazole
HeLa cell line
CDK2 enzyme
Cell cycle arrest
QSAR
Molecular docking

ABSTRACT

Motivated by the potential anticancer activity of both coumarin and 2-aminothiazole nuclei, a new set of thiazol-2-yl hydrazono-chromen-2-one analogs were efficiently synthesized aiming to obtain novel hybrids with potential cytotoxic activity. MTT assay investigated the significant potency of all the target compounds against the human cervical cancer cell lines (HeLa cells). Cell cycle analysis showed that the representative compound **8a** led to cell cycle cessation at G0/G1 phase indicating that CDK2/E1complex could be the plausible biological target for these newly synthesized compounds. Thus, the most active compounds (**7c and 8a-c**) were tested for their CDK2 inhibitory activity. The biological results revealed their significant CDK2 inhibitory activity with IC_{50} range of 0.022–1.629 nM. Moreover, RT-PCR gene expression assay showed that compound **8a** increased the levels of the nuclear CDK2 regulators P21 and P27 by 2.30 and 5.7 folds, respectively. ELISA tequnique showed also that compound **8a** led to remarkable activation of caspases-9 and -3 inducing cell apoptosis. QSAR study showed that the charge distribution and molecular hydrophobicity are the structural features affecting cytotoxic activity in this series. Molecular docking study for the most potent cytotoxic compounds (**7c and 8a-c**) rationalized their superior CDK2 inhibitory activity through their hydrogen bonding and hydrophobic interactions with the key amino acids in the CDK2 binding site. Pharmacokinetic properties prediction of the most potent compounds showed that the newly synthesized compounds are not only with promising antitumor activity but also possess promising pharmacokinetic properties.

1. Introduction

Cancer is a critical health problem characterized by uncontrolled mechanisms that direct cell proliferation and differentiation [1]. It results from intercellular and intracellular communication disorders initiated by false messages from hormones, cytokines, growth factors or by false signal transduction generated by oncogenes. The uncontrolled cell division and differentiation is strongly correlated to the activating or driving mutations in these oncogenes [2]. Due to these facts, as well as the possibility of cancer occurrence in various stages of development, there are many molecular targets for cancer therapy which can control the cell signaling pathways [3,4]. Among the extensively studied molecular targets are cyclin dependent kinases (CDKs) that exist in various isoforms [5]. CDKs constitute a family of serine/threonine protein kinases which are involved in numerous physiological processes as cell division, proliferation, apoptosis and gene transcription [6], in addition to their critical role in sustaining cancer cell proliferation [7]. Therefore, they are considered attractive therapeutic targets for identification of novel anticancer drugs. Among the different CDK subtypes, CDK2 received great attention; due to its involvement in various critical cellular processes upon complexation with its activating proteins, cyclin E or A [8]. Its complex with cyclin E enables sequential phosphorylation of the retinoblastoma protein (Rb) and activation of transcription factor E2F which initiates S phase [9]. On the other hand, association with cyclin A, permits continuous DNA replication and properly programed deactivation of E2F [10]. The importance of CDK2 as anticancer target is still in question, since the cdk2 knock-out mice are viable and CDK2 knockdown experiments failed to induce cell cycle cessation in a number of tumor cell lines [11]. However, there are many researches confirmed the overexpression of CDK2 in many malignancies as melanoma and lung, ovarian and pancreatic carcinoma [12]. Furthermore, current investigations using chemical genetic methods for maintaining

* Corresponding author.
E-mail address: yasmin_syam@yahoo.com (Y.M. Syam).

https://doi.org/10.1016/j.bioorg.2019.01.026
Received 13 July 2018; Received in revised form 18 December 2018; Accepted 16 January 2019
Available online 19 January 2019
0045-2068/

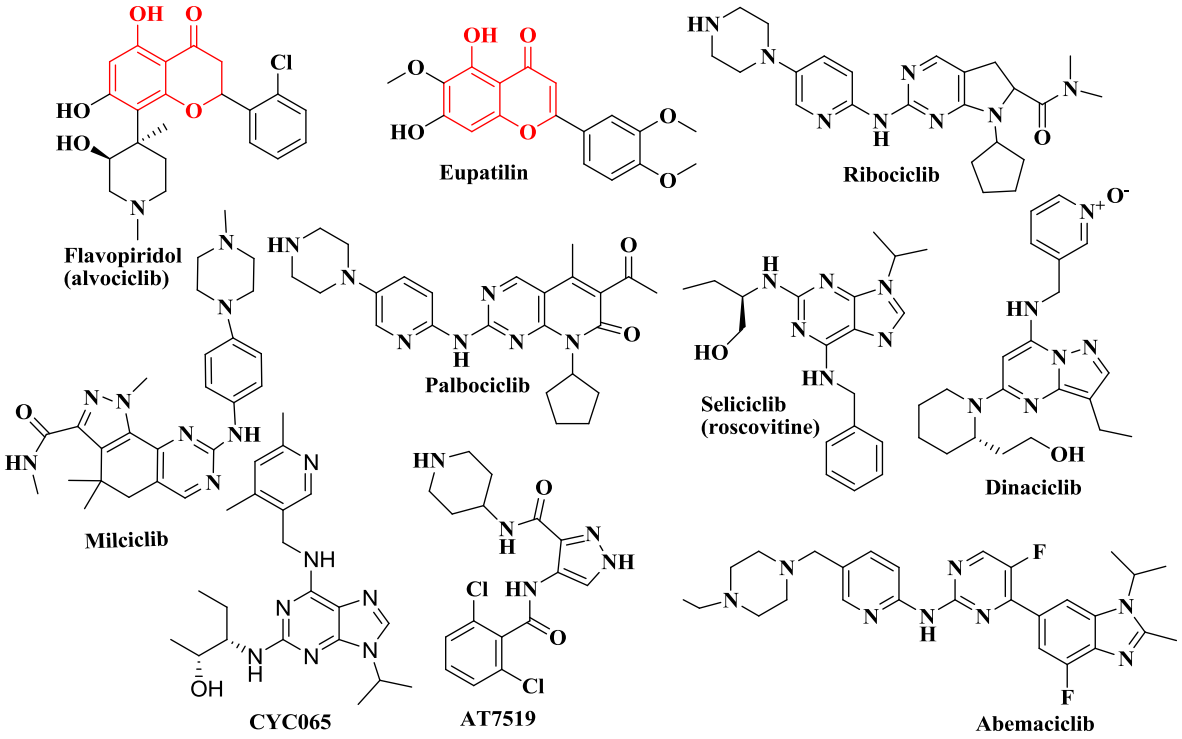

Fig. 1. Different examples of CDK2 inhibitors.

the CDK2 expression while inhibiting its activity afford an evidence for the validity of CDK2 as a potential anticancer drug target [13]. Currently there are many CDK2 inhibitors have entered clinical investigation [8] (Fig. 1).

Thiazole is a privileged scaffold in medicinal chemistry due to its numerous biological activities. It is the main building block in many potent drugs [14]. Moreover, many studies reported the inherited antitumor potency of many thiazole containing compounds [15–17]. Among them, the 2-aminothiazole analogs showed a prominent antitumor activity through the inhibition of different protein kinases [18–20]. The 2-amino-thiazole-5-carboxamide derivative **I** is a potent inhibitor of multiple Src-family members (Src kinase K_i = 96 pM) [18]. In addition, the 2-acetamide-thiazole derivative **II** possesses a high potency and selectivity towards CDK2 (IC_{50} = 0.17 μM) [16], the 2-amino-thiazole derivative **III** exhibited a potent CDK2 inhibitory activity as an ATP antagonist with promising anticancer activity against HeLa cell line [21]. Finally, the 2-acetamido derivative **IV**, (BMl-259), is regarded as a potent inhibitor for CDK2 and CDK5 with IC_{50} in the nano mole ranges [21] (Fig. 2).

Also, depending on protein data bank (PDB ID: 3QTR) [22], co-crystallization of (4-amino-2-(phenylamino)thiazol-5-yl)(phenyl)methanone (RC-1-148) as an inhibitor with CDK2 protein kinase produced its inhibition effect via the occupation of the thiazole ring the region which fits the ATP purine ring, in addition to three hydrogen bond interactions between the diaminothiazole moiety and the key amino acids Glu81 and Leu83 as will be further discussed in details under molecular docking section.

The cancer chemopreventive activity of various synthetic and natural chromones and their coumarin isoster derivatives as potent cytotoxic and cytostatic agents has been widely confirmed [23,24]. Their activities extend to several mammalian cancer cell lines *in vitro* and in xenograft models [25]. Their cytotoxic activity is exerted through various mechanisms as: inhibiting free radical injury [26], blocking cell cycle in G0/G1 [27] or in G2/M [28] phase, induction of caspase-9 mediated apoptosis and modulating estrogen receptor (ER) [29]. In addition, the inhibiting activities of different protein kinases, tolemerase enzyme and the DNA replication associated proteins as topoisomerase were also reported by different coumarin analogs [30,31].

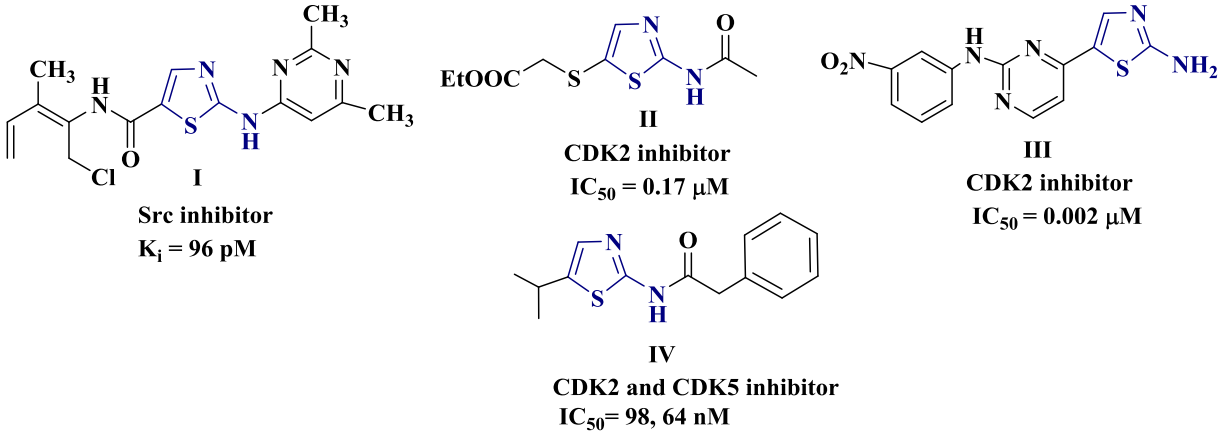

Fig. 2. Various 2-amino-thiazole derivatives with reported kinase inhibitory activity.

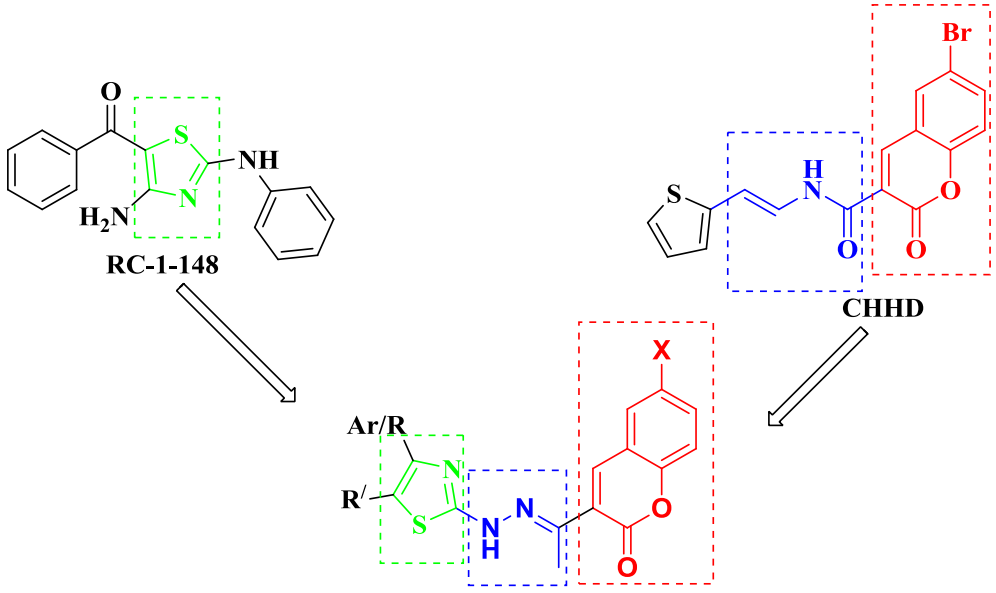

Fig. 3. Design strategy of the newly synthesized compounds.

Flavopiridol (Alvocidib) (Fig. 1), is one of the first generation of pan-CDKs inhibitors with anti-tumor activity attributed to down-regulation of CDK9-mediated anti-apoptotic proteins, especially Mcl-1 [32]. Eupatilin, a natural flavone compound, causes down-regulation of the expression of cyclin D1 in *ras*-Transformed Human Breast Epithelial (MCF-10A-ras) cells. It leads to the reduction in c-Jun expression and DNA binding activity of AP-l transcription factor which is an important factor in the cell cycle arrest of ras-transformed breast epithelial cells [33] (Fig. 1).

Furthermore, Nasr et al. [23] revealed that the coumarin hydrazide hydrazone derivative CHHD led to down-regulate kinase enzymes including CDK2 (Fig. 3). In addition, the hydrazone moiety is a promising linker in medicinal chemistry as many recent reports confirmed its ability to enhance the anticancer activity of various designed series via its NH binding to the target enzymes by hydrogen bonding and/or its behaving as an aza substituted amino acid surrogate [34,35].

In the light of the previously mentioned facts and in continuation of our different studies to synthesize new potent anticancer agents with high therapeutic index [36], this study is focused on the design and synthesis of new hybrid derivatives carrying coumarin nucleus conjugated with thiazole ring via ethyl hydrazone linker aiming to synergize their anticancer activity (Fig. 3). The cytotoxicity of all the target compounds was examined against HeLa cell line in comparison to doxorubicin using MTT assay. The most potent compounds were also subjected to CDK2E1 enzyme assay to evaluate their enzyme inhibitory effect. For further investigation of the different plausible cellular mechanisms of action, studies on cell cycle, cell apoptosis and the levels of caspase-3 and caspase-9 using flow cytometry technique were carried out on a representative compound. Quantitative structure–activity relationship (QSAR) study for the active set of compounds was carried out to investigate the structural features which influence their cytotoxic activity and to provide the mental picture required to improve the activity of this series. Molecular docking study of the most active compounds was also performed to find out the plausible binding modes of the newly synthesized compounds with CDK2 binding site, and to study their interaction with the protein hot spots (key amino acids). Finally, the physicochemical, pharmacokinetic and drug-likeness properties of the most potent compounds were examined *in silico*.

2. Results and discussion

2.1. Chemistry

The synthetic strategy for the construction of the target coumarin-thiazole hybrids **3–9** is illustrated in (Scheme 1). Substituted 3-acetylcoumarin **1a-c** were prepared by Knoevenagel condensation through the reaction of different substituted salicylaldehydes with ethyl acetoacetate in the presence of few drops of piperidine as a catalyst according to the reported method [37–40]. In absolute ethyl alcohol containing a catalytic amount of acetic acid, the obtained substituted coumarins **1a-c** were further converted into their corresponding thiosemicarbazone derivatives **2a-c** in good yields by their condensation with thiosemicarbazide [37,41,42].

Carbothioamides are versatile intermediates and so they were utilized here for the synthesis of the target functionalized coumarin-thiazole hybrids. In this context, the Hantzsch reaction [43] of 2-(1-(6-substituted-2-oxo-2*H*-chromen-3-yl)ethylidene)hydrazinecarbothioamides **2a-c** with different α-haloketones was carried out. Thus, the derivatives **2a-c** were treated with the α-haloketones namely; chloroacetone, phenacyl bromide, 4-bromo-phenacylbromide and/or 2-bromoacetyltetralin in refluxing ethanol in the presence of a catalytic amount of anhydrous sodium acetate to afford the 4-substituted thiazole-coumarin derivatives **3–6**, respectively. The spectral data and the elemental analyses were in consistent with the structures of the proposed compounds. The IR spectrum of 6-bromo-3-(1-(2-(4-(5,6,7,8-tetrahydronaphthalen-2-yl)thiazol-2-yl)hydrazono)ethyl)-2*H*-chromen-2-one (**6c**) as a representative example, showed strong absorption bands at 3427, 1730 cm^{-1} attributed to the NH and CO groups, respectively. While its ^{1}H NMR spectrum showed besides the expected aromatic signals, two new groups of multiple signals at δ1.68–1.74 and 2.71–2.75 ppm assigned to the eight protons of the tetrahydro-naphthalene ring in addition to one singlet signal at δ 2.10 ppm assigned to the methyl protons. The ^{13}C NMR spectrum displayed the most important signals at δ 17.39, 22.73, 29.25, 29.5 ppm characteristic for the CH_3 carbon and the four CH_2 carbons of tetrahydro-naphthalene, respectively (Supplementary data).

Furthermore, the reaction of the coumarin-thiosemicarbazone derivatives **2a-c** with 3-chloroacetylacetone and/ or ethyl-2-chloroacetoacetate produced the corresponding 5-acetyl and/ or ethyl

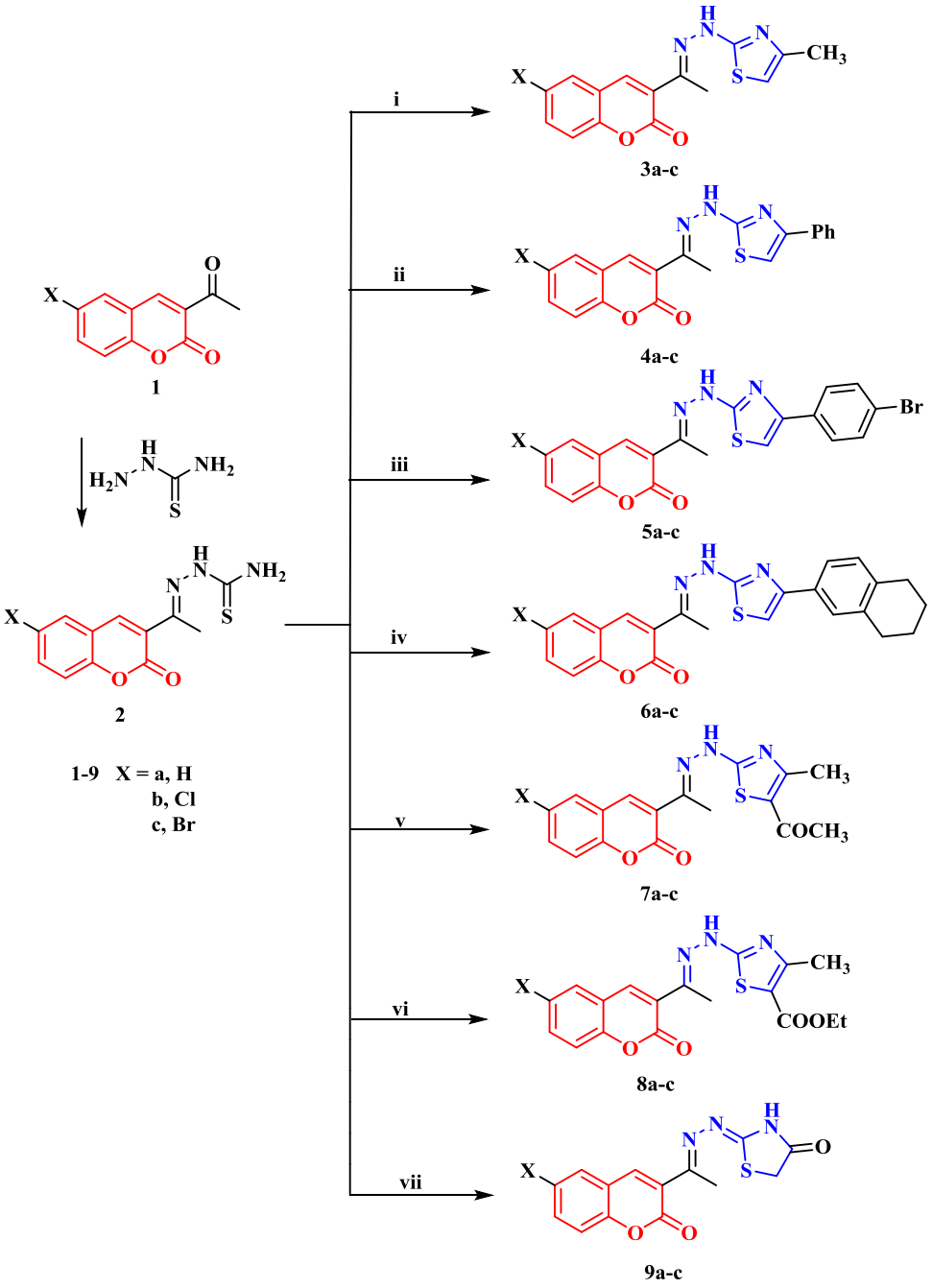

Scheme 1. Synthesis of new thiazol-hydrazono-chromen-2-one hybrids.

carboxylate thiazole analogs **7a-c** and **8a-c**, respectively. Spectral and elemental analyses confirmed the structures of the obtained derivatives. The ^{1}H NMR spectrum ascertained the structure of compound **7c** through displaying three singlet signals at δ 2.30, 2.41 and 2.54 ppm corresponding to the two methyl and one acetyl protons. Moreover, its ^{13}C NMR spectrum exhibited signals at δ 15.46, 17.94, 29.60 and 190.23 ppm due to the three methyl and one carbonyl carbons, respectively. Additionally, ^{1}H NMR spectrum of compound **8b** showed two singlet signals at δ 2.34, 2.72 ppm representing the two methyl protons, while the presence of the ethyl ester group was confirmed by the appearance of one triplet and another quartet signals at δ 1.35 and 4.31 ppm, respectively. The ^{13}C NMR spectrum of the same compound exhibited signals at δ 14.40, 60.80 and 169.00 ppm related to the ester carbons besides another two signals at 14.97 and 17.20 ppm referring to the two methyl carbons. Finally, the treatment of **2a-c** with ethyl bromoacetate afforded the coumarinthiazolidin-4-one derivatives **9a-c**. Mass spectra of the obtained analogs revealed the molecular ion peaks of the compounds in agreement with their structural formulae (Scheme 1).

2.2. Biological Screening

2.2.1. In vitro anticancer activity

Various biological studies reported that the tumor suppressor genes P16, P21 and P27 prevent cell cycle progression by direct interfering with cyclin/cyclin-dependent kinase (CDK) activation [44]. These genes are potent inhibitors of CDK, and it has been reported that the aberrant expression of these nuclear gene products leads to CDKs overexpression and neoplastic development in several cancer types such as cervical carcinoma [44,45]. Accordingly, the cytotoxic activity of all

Table 1
In-vitro antiproliferative activity of the new thiazol-2-yl-hydrazono-chromen-2-one derivatives against Hela cell line.

Compounds	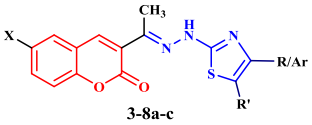 3-8a-c			Antiproliferative activity IC_{50} (cM)
	X	R/Ar	R'	
3a	H	CH_3	H	1.6369 ± 0.0097
3b	Cl	CH_3	H	0.1807 ± 0.0029
3c	Br	CH_3	H	0.4288 ± 0.0041
4a	H	Ph	H	n.d
4b	Cl	Ph	H	0.2055 ± 0.0019
4c	Br	Ph	H	n.d
5a	H	*p*-Br-Ph	H	0.1401 ± 0.0043
5b	Cl	*p*-Br-Ph	H	0.2254 ± 0.0055
5c	Br	*p*-Br-Ph	H	0.9437 ± 0.0021
6a	H	Tetralin	H	n.d
6b	Cl	Tetralin	H	n.d
6c	Br	Tetralin	H	n.d
7a	H	CH_3	$COCH_3$	0.2862 ± 0.0069
7b	Cl	CH_3	$COCH_3$	0.5689 ± 0.0031
7c	Br	CH_3	$COCH_3$	0.0654 ± 0.0038
8a	H	CH_3	COOEt	0.0596 ± 0.0026
8b	Cl	CH_3	COOEt	0.0236 ± 0.0011
8c	Br	CH_3	COOEt	0.0091 ± 0.0007
	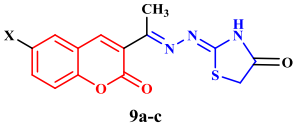 9a-c			
9a	H			0.6306 ± 0.0016
9b	Cl			1.5993 ± 0.0091
9c	Br			0.3156 ± 0.0030
Dox.				1.1073 ± 0.0062

IC_{50} values were determined in triplicate in range of 0 (control) to 100 μM. IC_{50} means the concentration (μM) that inhibits the growth of 50% of cell during a three day cultivation.

the target compounds was evaluated *in vitro* against human cervical carcinoma cell line (HeLa cells) in comparison to doxorubicin as a reference drug using MTT assay [46,47]. Furthermore, the compounds showed potent cytotoxic activity were evaluated as CDK2 inhibitors using ADP-Glo™ Kinase Assay. To assess the influence of this series of compounds on the levels of the tumor suppressor genes, a representative compound for this series was further undergone P21 and P27 expression assay.

In the view of the obtained data (Table 1), most of the tested derivatives produced significant antiproliferative activity that is more or equipotent to that of doxorubicin. These results confirmed the efficiency of the thiazole-hydrazonoethyl-chromen-2-one scaffold in producing the desired anticancer activity. It is obvious that the structural variations in the substituents attached to the parent scaffold affected the activity significantly. According to Table 1; the 6-bromo-coumarin derivative (**8c**) exhibited the highest cytotoxic efficacy about 100 folds more potent than that of the reference doxorubicin (IC_{50}; 0.009 *vs* 1.10 μM). A remarkable reduction in the potency was observed by the 6-chloro-coumarin analog (**8b**) and the unsubstituted coumarin derivative **8a** (IC_{50}; 0.024 and 0.059 μM, respectively). Nevertheless, the potency of both derivatives was still higher than doxorubicin by 55 and 18 folds, respectively. This indicated that the increase in the hydrophobicity of the substituent at coumarin-C6 position enhances the anticancer activity. Replacement of the ethyl ester at the thiazole-C_5 in (**8a-c**) with an acetyl moiety in (**7a-c**) led to further drop in the potency (IC_{50} 0.065–0.56 μM). Interestingly, despite the detectable reduction in the cytotoxic activity of **7a-c**, their efficacy is much more potent than the reference drug. Likewise, the unsubstituted analogs at the thiazole-C_5 (**3a-c**) produced less anticancer activity than the previous derivatives but still more or equipotent to that of the reference doxorubicin with IC_{50}; 0.18–1.63 μM. Furthermore, the significant sensitivity of the HeLa cells in comparison to doxorubicin was still detected upon replacement of the CH_3 group at the thiazole-C_4 with a phenyl or *p*-Br-phenyl moiety (**4b** and **5a-c,** respectively) giving IC_{50}; 0.14–0.94 μM. Unfortunately, complete loss of activity was detected by the unsubstituted phenyl derivatives (compounds **4a,c**) and also upon increasing the ring sizes of the attached moieties at the thiazole-C4 such as tetrahydro-naphthalene ring (compounds **6a-c**), this may be due to steric clashes with the CDK2 binding site, *vide infra* in the molecular docking section. Although, the anticancer activity of the thiazolidinone analogues **9a-c** was more potent or equivalent to that of doxorubicin (IC_{50}; 0.31–1.59 μM), there was a dramatic reduction in the potency when compared with that of the thiazole derivatives **8a-c**. It is apparent from the obtained biological data that the structural variations in the substitution pattern on the thiazole ring leads to a detectable fluctuation in the anticancer potency. Based on the previous discussion, it could be concluded that the thiazol-2-yl-hydrazono-chromen-2-one scaffold is a favorable nucleus for discovering new potent anticancer agents against HeLa cell line (Fig. 4).

2.2.2. Cellular mechanism of action

One of the most active compounds **8a** was used as a representative for the newly synthesized compounds for the detailed cellular mechanistic investigation of their effect on cell cycle progression to pinpoint their plausible biological target. Inspection of the results showed that the tested compound induced accumulation of cells at G0/G1 phase by 62.19% (Fig. 5.**A**) in comparison to 37.23% by Doxorubicin (Fig. 5.**C**) Table 2. Thus, compound **8a** led to cell cycle cessation in G1 phase preventing DNA synthesis. It has been reported that the CDK2 pathway plays an important role at G1 phase upon complexation with cyclin E and its inhibition arrests cell cycle progression at G0/G1 phase preventing DNA synthesis [9], thus CDK2/E1 complex could be the biological target for the newly synthesized compounds.

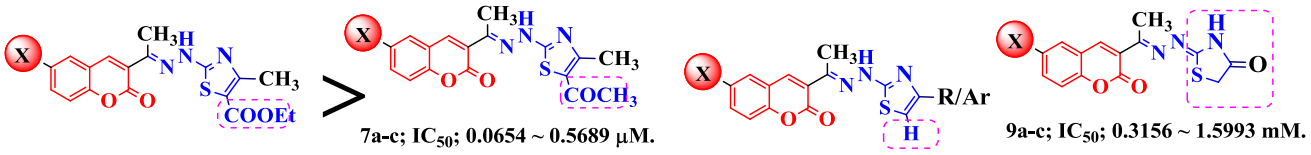

Fig. 4. The anticancer activity of the new thiazole-coumarin derivatives.

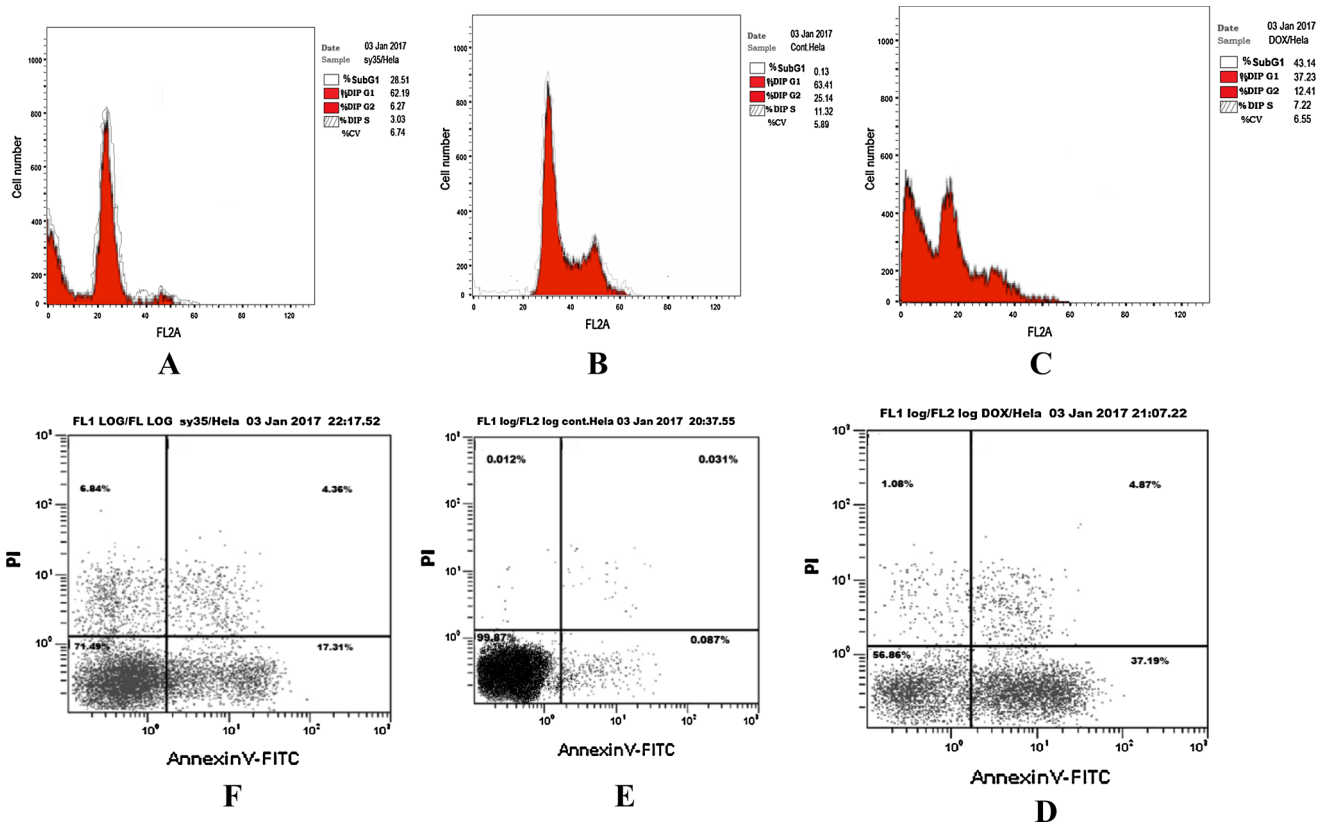

Fig. 5. Cellular mechanism of action of compound **8a**.

Table 2
Cell cycle analysis for compound **8a**.

Sample Code	IC_{50}uM	%G0-G1	%S	%G2-M	% Apoptosis
8a	0.0596 ± 0.0026	62.19	6.27	3.03	28.51
Dox	1.1073 ± 0.0062	37.23	7.22	12.41	43.14
Control HeLa		63.41‘	25.14	11.32‘	0.13

2.2.3. *In vitro CDK2E1 assay*

Many studies confirmed that CDK2 is overexpressed in uterine cervical carcinoma cells [44,45], thus, the compounds represented the most potent anticancer activity (**7c** and **8a-c**) were selected as representatives to study the CDK2 inhibitory activity of this series and the results were tabulated in table 3. All the examined compounds produced significant inhibitory activity against the target enzyme CDK2/E1 with IC_{50} in the nano-mole range compared to staurosporine as reference compound (Table 3). Interestingly, the most potent cytotoxic derivative **8c** showed the most potent enzyme CDK2/E1 inhibitory activity twice that of the reference compound ($IC_{50;}$ 0.022 *vs* 0.044 nM). Apparent decrease in the target enzyme inhibition was detected by the 6-chloro and the unsubstituted coumarin analogues **8b** and **8a** less than that of the reference compound ($IC_{50;}$ 0.216, 1.629 nM, respectively). As noticed, the order of their CDK2 enzyme inhibition agrees well with their cytotoxic activity order confirming that the CDK2 inhibition is the main mechanism of action for this series of newly synthesized compounds. The replacement of the 5-thiazole carboxylate group with acetyl group in **7c** did not produce significant impact on the inhibition activity ($IC_{50;}$ 1.546 nM). In the view of the obtained results, the attached bromine moiety at coumarin-C_6 displayed a central role in exhibiting significant anticancer potency against Hela cell lines by targeting CDK2E1 enzyme (Fig. 6).

Table 3
In-vitro CDK2/E1 assay of the most potentthiazol-2-yl-hydrazono-chromen-2-one derivatives.

Compounds	CDK2/E1 inhibition activity IC_{50} (nM)
7c	1.546 ± 0.021
8a	1.629 ± 0.012
8b	0.216 ± 0.014
8c	0.022 ± 0.002
Staurosporine	0.044 ± 0.002

IC_{50} values were determined in triplicate in the range of 0.01 to 10 nM. IC_{50}value indicates concentration (nM) that inhibits activity of the tested enzyme to 50%.

2.2.4. *RT-PCR gene expression assay*

The representative **8a** was tested in a reverse transcription polymerase chain reaction (RT-PCR) gene expression assay at its IC_{50} concentration to investigate its effect on the levels of the CDK nuclear suppressors P21 and P27 in addition to its effect on CDK2/A1 isoform. As illustrated in Table 4, in comparison to the control, compound **8a** increased the level of the tumor suppressor proteins P21 and P27 by 2.360 and 5.758 folds, respectively that could participate in its CDK2 down regulation. While the level of CDK2/A1 enzyme was decreased by 0.404 fold.

2.2.5. *Apoptosis induction and Caspase- 3 and -9 levels.*

It has been reported that the induction of apoptosis and permanent removal of neoplastic cells are important for efficient cancer chemotherapy [46–49]. So, various studies have investigated the induction of apoptosis upon efficacious cancer treatment [50]. A representative compound **8a** was used to investigate the apoptotic effect of the series in HeLa cell line.

In order to investigate whether apoptosis attributes to the antiproliferative effect of the thiazole derivative **8a**, annexin V/propidium iodide (PI) staining of HeLa cell line was performed upon incubation for

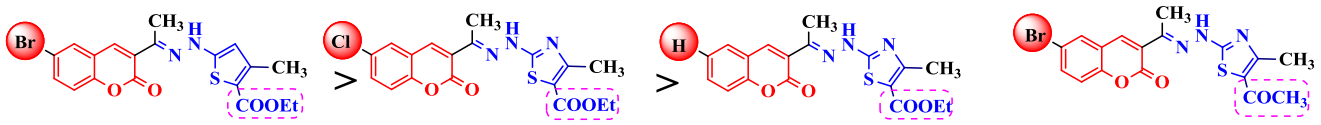

Fig. 6. CDK2/E1 inhibitory activity of the new thiazole-coumarin derivatives.

Table 4
RT-PCR gene expression assay for compound **8a**.

Sample Code	P21 Fold	P27 Fold	CDK2/A1 Fold
8a	+2.360	+5.758	−0.404
Control	1	1	1

24 h (Fig. 5. **D**) in comparison to dil., DMSO as a negative control (Fig. 5. **E**) and Doxorubicin as a positive control (Fig. 5. **F**). The tested compound induced more apoptotic cells (annexin V+/PI− and annexin V+/PI+) producing apoptosis percentage of 28.50% *vs* 0.13% for DMSO. The percentage of cells undergoing apoptosis is defined as the sum of early apoptotic (annexin V+/PI−) cell percentage and late apoptotic (annexin V+/PI+) plus necrosis cell percentage.

It is noteworthy that the activation of caspases is the best recognized hallmark of apoptosis. The caspase cascade events precisely mediate the induction of apoptosis via either intrinsic or extrinsic pathways [48,49]. The importance of caspase-3 in the induction of apoptosis resulted from its participation in cell shrinkage, chromatin condensation, and DNA fragmentation [48]. On the other hand, caspase-9 is activated during intrinsically triggered apoptosis at the apoptosome [49]. Consequently, the sensitive and reproducible detection of active caspase-3 and -9 is very essential in understanding of cellular functions and multiple pathologies of etiologies [51]. Using ElISA assay kit, the bioluminescent intensities of caspases-3 and -9 were measured time-dependently in HeLa cells treated with IC_{50} concentration of **8a** for 24 h of treatment. As demonstrated in Table 5, a significant increase in the levels of capases-3 and -9 was noticed in **8a** treated cells after 24 h of incubation in comparison to doxorubicin as a reference drug. Therefore these results show that the newly synthesized series are apoptotic inducers.

2.2.6. Effect of the most active compound against human normal lung cell line WI 38

In order to determine the safety profile of the tested compounds, the most active target analog against the cervical cancer cell line HeLa (**8c**) was selected as a representative example to be examined against the human normal lung cells (WI 38) and its IC_{50} was determined via MTT assay. Fortunately, the IC_{50} of the tested compound against the normal cells was higher than its IC_{50} dose against cancer cell line (8 fold) (0.075 ± 0.0023 µM *vs* 0.0091 µM, respectively). This result reflects the requirement of more derivatization and optimization for this scaffold to produce more safe analogs of high therapeutic index with potential cytotoxic activity.

Table 5
Caspases -3, -9 concentrations in HeLa cells after treatment with compound **8a** or Doxorubicin for 24 h.

Compound	Caspase 3 conc. (Pg/mL)	Caspase 9 conc (ng/mL)
8a	1806	74.55
DOX	1296	59.72
Control (HeLa)	29.1	2.06

3. Molecular modeling study

3.1. Quantitative structure–activity relationship (QSAR) study

QSAR study was performed to investigate the structural features influencing the cytotoxic activity of the newly synthesized compounds and the structural variations which could be exploited for structure optimization.

The 16 newly synthesized compounds were divided into a training set of 13 compounds and a test set of 3 compounds such that the test set maintains the activity value distribution of the original dataset. The experimental cytotoxicity IC_{50} were converted to pIC_{50} (-log IC_{50}) for mathematical convenience. A pool of 313 molecular mechanical descriptors available in Molecular Operating Environment (MOE, 10.2008) software QSAR module was calculated for the training set.

The obtained "descriptors-target property" matrix was then used in Rapid Miner 7.1.000 Basic Edition for QSAR model generation [52–54]. Descriptor filtration was first carried out by the removal of the redundant descriptors "low variance descriptors", which add no additional information to the model, leaving 286 descriptors for model generation. Multiple Linear Regression (MLR) was used as the machine learning algorithm for the generation of a linear model which is characterized by simplicity, transparency and interpretability. Descriptor selection was then carried out using the classical forward selection algorithm (FSA) available in Rapid Miner [55]. In the performed FSA, Root mean square error of a leave-one-out (LOO) cross-validation ($RMSE_{CV}$) was used for model performance evaluation. The first descriptor included in the regression is the one that gave the highest one-descriptor model performance (lowest $RMSE_{CV}$). Then unused descriptors were gradually added to the regression, only the descriptor gave the highest increase in performance (lowest $RMSE_{CV}$) was added to the selected descriptor pool at a time. The training stopped when the addition of a further new descriptor did not improve the model performance (did not reduce $RMSE_{CV}$ further).

$$pIC_{50} = -40.577 * (BCUT\_PEOE\_0) - 0.092 * (vsurf\_DW12) - 86.794 \quad (1)$$

Based on the FSA a two-descriptors model was generated (**Eq. (1)**) with a significantly good performance as represented in its statistical evaluation parameters and its predictions (Table 6 and Table 7) where its coefficient of determinations R^2 for training set prediction and cross-validation are 0.907 and 0.879, respectively, with root mean square error RMSE of 0.377 and 0.438, respectively. The proximity between the training set prediction and cross-validation results indicates the robustness of the model and its lack of overfitting.

Fig. 7 shows the excellent correlation between the experimental and

Table 6
Statistical performance of the QSAR model in training and test set prediction and in leave-one-out (LOO) cross-validation.

	Training set prediction	LOO_{CV} prediction	Test set prediction
R^2	0.907	0.879	0.905
RMSE	0.377	0.438	0.398

Table 7
Experimental and predicted cytotoxicity pIC_{50} for the training set and test set compounds and the training set prediction in LOO_{CV} and the calculated residual error in the different cases.

MolID	Experimental pIC_{50}	Training set prediction	Residual error[a]	LOO_{CV} prediction	Residual error[a]
3a	5.786	6.737	−0.951	6.860	−1.075
3b	6.743	6.623	0.120	6.608	0.135
3c	6.368	6.018	0.350	5.800	0.568
4b	6.687	6.615	0.072	6.606	0.081
5a	6.853	6.711	0.143	6.694	0.159
5b	6.647	6.615	0.032	6.611	0.036
7b	6.245	6.012	0.233	5.880	0.365
8a	9.569	9.295	0.273	9.124	0.444
8b	8.097	8.669	−0.571	8.328	−0.230
8c	9.620	9.295	0.324	9.092	0.527
9a	6.200	6.253	−0.053	6.261	−0.060
9b	5.796	6.110	−0.314	6.163	−0.367
9c	6.501	6.159	0.341	6.101	0.400
MolID	*Experimental pIC_{50}*	*test set prediction*	*residual error[a]*		
5c	6.025	6.011	0.014		
7a	6.543	6.112	0.431		
7c	7.184	6.646	0.538		

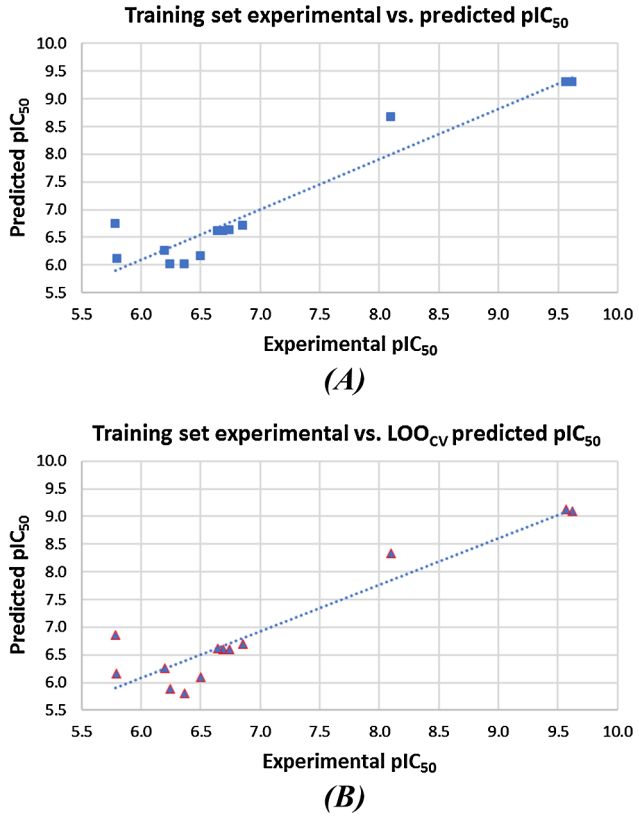

Fig. 7. Correlation plot for (a) training set experimental *vs.* predicted pIC_{50} and (b) training set experimental *vs.* LOO_{CV} predicted pIC_{50}.

model predicted biological activity in training set prediction and in LOO cross-validation.

For further model validation to ensure that it predicts the data points and not just fits them, the model was used to predict the biological activity of the unseen test set compounds. The model showed significantly good prediction of the test set biological activity (Table 6 and Table 7) as represented in its R^2 of 0.905 and RMSE of 0.398 indicating the robustness and the predictive ability of the obtained QSAR model.

The two descriptors selected in the model are *BCUT_PEOE_0* and *vsurf_DW12* and they are both inversely proportional to the biological activity (with negative coefficients). BCUT_PEOEs* are 2D descriptors calculated from the eigenvalues of a modified adjacency matrix using atomic contribution to partial charge, so, they describe the molecular atomic partial charge distribution [56]. BCUT_PEOE_0 represents the smallest eigenvalue. Vsurf_DWs* are 3D molecular descriptors similar to the VolSurf descriptors which represent the distances (energy difference) between the best three local energy minima (the three lowest interaction energies) when a water probe interacts with the ligand, so, they describe the molecular hydrophilicity [57]. Vsurf_DW12 represents the energy distance between the lowest and 2nd lowest energy minima.

In summary, the QSAR indicates that the structural features affect the cytotoxicity in this series are the molecular partial charge distribution and so its impact on the molecule's ability to perform electrostatics-dependent interactions (like H-bonding) [*vide infra* in molecular docking results and discussion] and hydrophilicity which is inversely proportional to cellular cytotoxicity which is in line with the chemical intuition where decreased hydrophilicity indicates better cellular absorption and so better activity.

3.2. Molecular docking study

Molecular docking study was performed to understand the binding mode of the most potent compounds **7c** and **8a-c** to investigate their interactions with the key amino acids (hot spots) in the active site of the CDK2 enzyme with the aim of explaining their promising inhibitory activity.

More than 200 crystal structures are available in the protein data bank for CDK2 co-crystallized with an inhibitor [58]. In the current work, we used (PDB ID: 3QTR) [22,59] which has CDK2 co-crystallized with the diaminothiazole derivative RC-1-148 (IC_{50} = 0.93 μM) as inhibitor. As a protein kinase, CDK2 contains the conserved kinase core of a smaller *N*-terminal lobe that is almost β-sheets and a mostly α-helical larger C-terminal lobe with the ATP binding site located between these two lobes [60–62]. In case of CDK2, the key amino acids (hot spots) in the ATP binding pocket involved in the ATP binding are Thr14, Lys33, Glu81, Leu83 and Asp145 [63]. As can be seen in Fig. 8, the diaminothiazole derivative RC-1-148 blocks the ATP-binding pocket with its thiazole ring occupying part of the region which fits the ATP purine ring (the region accommodating the pyrimidine fragment of the purine ring). Through 3 hydrogen bond interactions the diaminothiazole moiety interacts with the key amino acids Glu81 and Leu83. This orientation of the thiazole ring fits the amino-phenyl moiety in position 2 in proximity of the amino acids Phe82 and Ile10 achieving hydrophobic interaction with their hydrophobic side chains. On the other side of the thiazole ring the benzoyl moiety in position 5 forms a water-mediated hydrogen bond with the Asp145 backbone NH.

Validation of the molecular docking protocol was first performed by re-docking of the co-crystallized ligand (RC-1-148) in the CDK2 active site. The re-docking validation step reproduced the experimental binding pattern of the co-crystallized ligand efficiently indicating the suitability of the used docking setup for the planned docking study as demonstrated by the small RMSD of 0.509 Å between the docking pose and the co-crystallized ligand (energy score (S) = −11.11 kcal/mol) and by its ability to reproduce all the key interactions accomplished by the co-crystallized ligand with the key amino acids (hot spots) in the active site (Glu81, Leu83 and Asp145) (Fig. 8).

According to the performed docking study, the most potent compounds **7c** and **8a-c** showed a common predicted binding pattern in the ATP binding site (Fig. 9 and supporting material **Figures S1-S3**) with their thiazole ring accommodated in the same region as that of the co-crystalized CDK2 inhibitor RC-1-148 in the purine binding region. Through two hydrogen bond interactions the 2-aminothiazol moiety interacts with the key amino acid leu83 backbone. Like RC-1-148, they

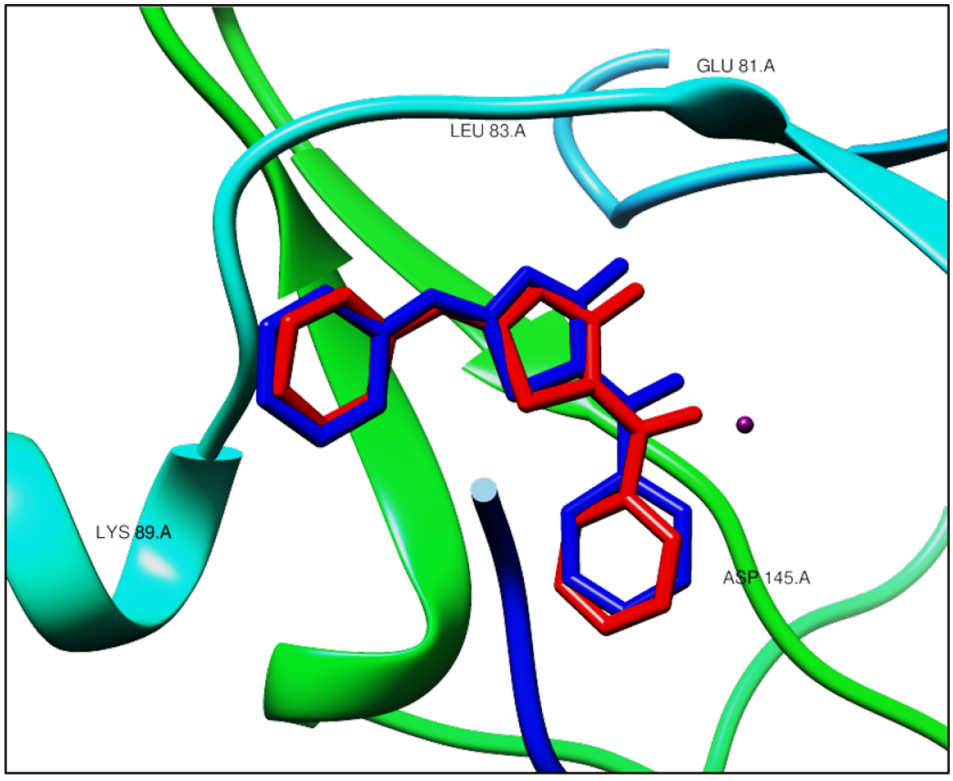

(A)

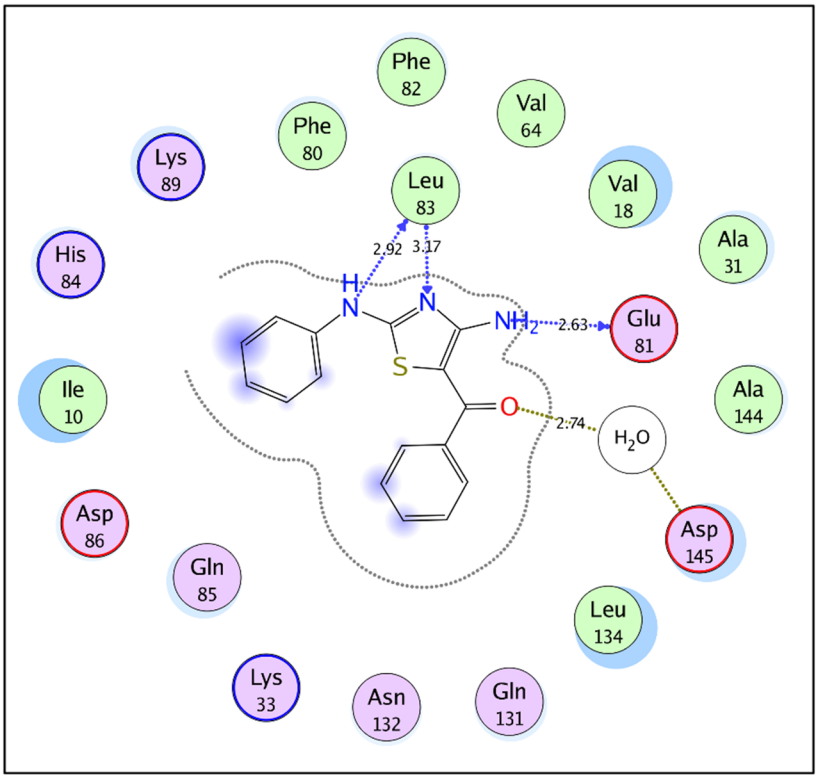

(B)

Fig. 8. (a) Superimposition of the docking pose (red) and the co-crystallized (blue) of RC-1-148 in the CDK2 active site with RMSD of 0.509 Å (A water molecule is in magenta and hydrogen atoms were removed for better visibility). (b) 2D interaction diagram showing RC-1-148 docking pose interactions with the key amino acids in the CDK2 active site. (Distances in Å).

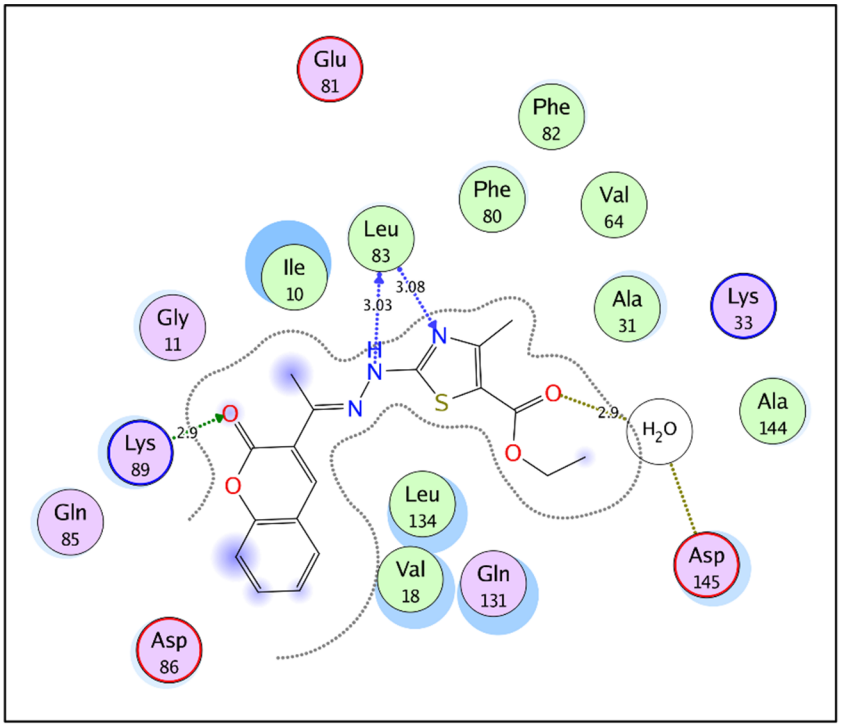

(A)

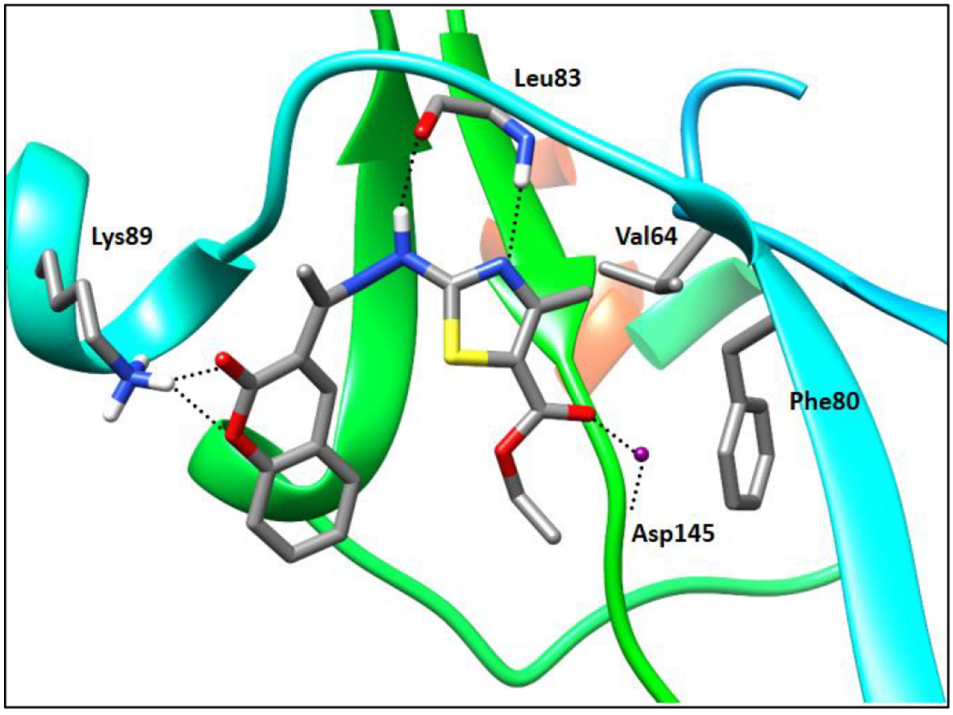

(B)

Fig. 9. 2D diagram (A) (Distances in Å) and 3D representation (B) of compound **8a** showing its interaction with the CDK2 active site (A water molecule in magenta).

form a water-mediated hydrogen bond with the key amino acid Asp145 backbone NH using their carbonyl group in position 5 of the thiazole ring. In addition to the interactions they share with RC-1-148, compounds **7c** and **8a-c** achieve further interactions with the ATP binding site, as they interact with their coumarin ring through hydrogen bonding with Lys89 NH_3^+ and through hydrophobic interaction with the hydrophobic side chains of Ile10, Val18, and Gln85 what rationalizes that the bromo substitution at the coumarin nucleus gives the highest cytotoxic, CDK2 inhibitory activity and Docking score (Tables 1, 3 and 8) and that the activity decreases with the decrease in the hydrophobicity of the substituent on the coumarin ring.

The methyl group on position 4 of the thiazole ring is fitted in the vicinity of the hydrophobic side chains of the amino acids Ala31, Val64 and Phe80 achieving a hydrophobic interaction with these side chains.

Table 8
Docking energy scores (*S*) in kcal/mol for the newly synthesized compounds **7c**, **8a-c** and the co-crystalized compoundRC-1-148in CDK2 active site.

Compound	Energy score (*S*) kcal/mol
RC-1-148	−11.11
7c	−13.03
8a	−13.00
8b	−13.42
8c	−13.66

Increasing the ring size of the attached moiety at the thiazole-C4 as tetrahydro-naphthalene ring in compounds (**6a-c**) abolishes the activity; this may be due to steric clashes with the CDK2 binding site.

This achieved binding pattern rationalizes the superior CDK2 inhibitory activity of these compounds as demonstrated in their experimental CDK2 enzyme assay results (Table 3) and their better binding affinity (docking score) relative to the co-crystalized RC-1-148 inhibitor (IC_{50} = 0.93 µM) [63] (Table 8).

3.3. Physicochemical, ADME and pharmacokinetic properties prediction

Swiss ADME web tool available from the Swiss Institute of Bioinformatics (SIB) was used for the calculation of the physicochemical descriptors as well as to predict the ADME parameters, pharmacokinetic properties and drug like nature of the most potent compounds **7c** and **8a-c** to ensure that these compounds are not only promising candidates in terms of biological efficacy but also from the pharmacokinetic aspects [64–67].

The tested compounds were found to possess promising physicochemical and pharmacokinetic properties. They showed a predicted log$P_{o/w}$ in the range of 3.53–4.10, moderate water solubility, high GIT absorption with no BBB permeability and so no predicted CNS side effects. (for more details see supporting materials).

Fig. 10 shows a BOILED-Egg graphical representation of the WLOGP *vs*. TPSA (topological polar surface area) for the tested compounds [64]. They located in the zone of human intestinal absorption (HIA) compounds with no BBB permeability; the graph shows also that they are not P-glycoprotein substrates (PGP−) so they are not liable to the efflux mechanism carried out by this transporter which is used by some tumor cell lines as drug-resistance mechanism [65].

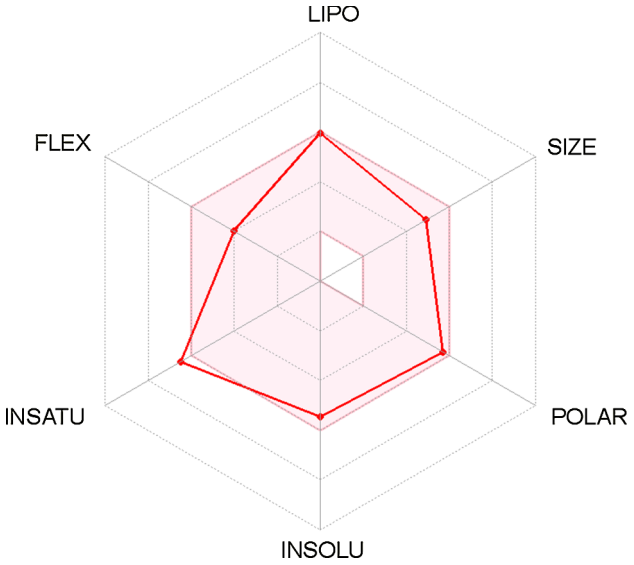

Fig. 11. Bioavailability radar chart from *swiss ADME* web tool for compounds **8c**. The pink area represents the range of the optimal property values for oral bioavailability and the red line is compound **8c** predicted properties.

The predicted high GIT absorption of the tested compounds is due to their optimum physicochemical properties located in the suitable physicochemical properties range for oral bioavailability. Fig. 11 shows the bioavailability radar chart for compound **8c** as a representative for the tested compounds. The radar plot bears six axes for six important properties for oral bioavailability; saturation (INSATU), size (SIZE), polarity (POLAR), solubility (INSOLU), lipophilicity (LIPO) and flexibility (FLEX) [66,67]. The range of the optimal property values is shown as a pink area and the red line represents compound **8c** predicted properties which is nearly fully included in the pink area indicating its good predicted oral bioavailability. (for bioavailability radar charts for compounds **7c, 8a** and **8b** see supporting materials **figures S4-S6**).

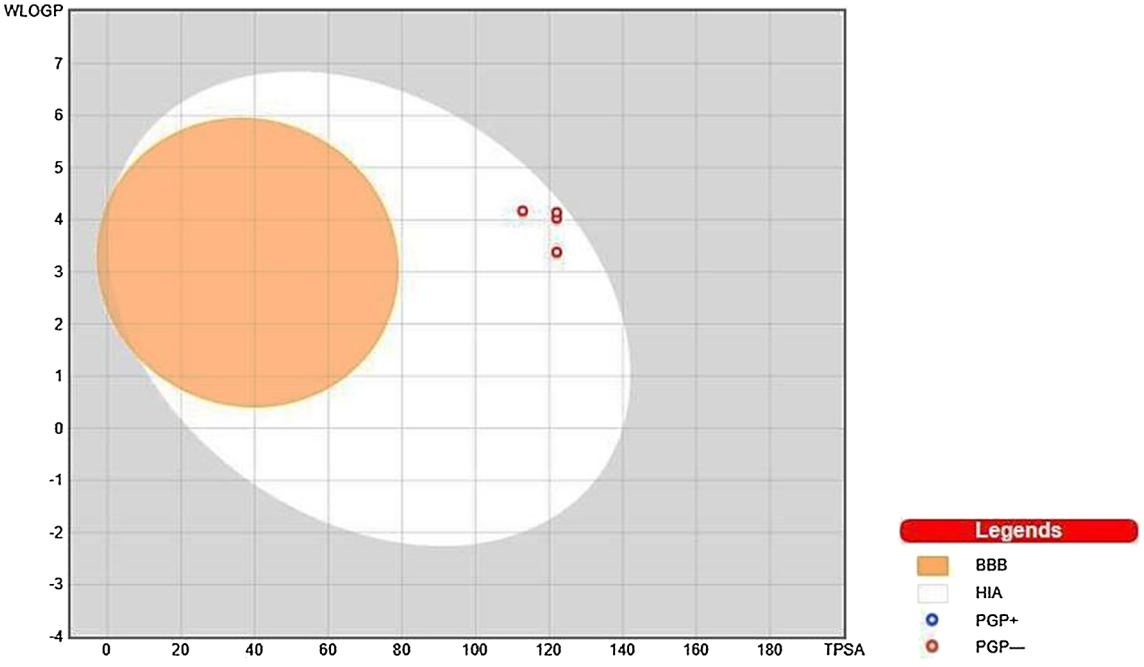

Fig. 10. Predicted Boiled-Egg plot from *swiss ADME* web tool for compounds **7c** and **8a-c**.

Swiss ADME web tool also showed that all tested compounds fulfil the drug likeness characteristics as defined by the major pharmaceutical companies; Lipinski (Pfizer) [68], the Ghose (Amgen) [69], Veber (GSK) [70], Egan (Pharmacia) [71] and Muegge (Bayer) [72] filters. Although it did not classify them as lead-like as their molecular weights exceeded 350 and their predicted log $P_{o/w}$ from XLOGP3 [73] model is higher than 3.5.

From the medicinal chemistry point of view *Swiss ADME* classified the test compounds as Non-PAINS (pan assay interference compounds) so, they are not frequent hitters or promiscuous compounds as they do not contain substructures showing potent response in assays irrespective of the protein target [74,75].

In summary, this *in Silico* study of the physicochemical and pharmacokinetic properties of the most potent compounds **7c** and **8a-c** showed that they are not only with promising biological activity but also with promising pharmacokinetic properties.

4. Conclusion

Novel hybrids of thiazole-hydrazonoethyl-chromen-2-one were synthesized and evaluated for their antiproliferative activity against HeLa cell line. Most of the tested compounds revealed more or equipotent cytotoxic activity to that of doxorubicin, especially the 5-acetyl-4-methylthiazol-chromenone derivative **7c** and the 4-methyl-2-oxo-chromen-3yl-thiazole-5-carboxylate derivatives **8a-c** producing IC_{50} values of range 0.0091–0.0654 μM compared to the reference doxorubicin with IC_{50}; 1.107 μM. Cellular mechanistic studies of compound **8a** as a representative example compound on HeLa cells showed that this compound induces accumulation of cells at G0/G1 by 62.19% in comparison to 37.23% by doxorubicin indicating that CDK2/E1 complex could be the plausible biological target for these newly synthesized compounds. Thus, CDK2/E1 assay was carried o-lkut for the most promising cytotoxic agents (**7c** and **8a-c**) proving their inhibitory efficiency against the target enzyme with IC_{50} ranging from 0.022 to 1.629 nM. The representative compound **8a** showed an enhancement effect on the level of the tumor suppressing proteins P21 and P27 by 2.30 and 5.7 folds, respectively on the contrary to its reduction influence on CDK2/A1 as proven using RT-PCR gene expression assay. Moreover, it showed apoptosis-inducing effect through the activation of caspases-3 and -9. QSAR study of the tested compounds displayed excellent correlation between the experimental and model predicted biological activity in the training set prediction and in the LOO cross-validation with high predictive power R^2 of 0.907 and 0.879, respectively, and low RMSE of 0.377 and 0.438, respectively. Moreover, the QSAR study showed that the charge distribution and molecular hydrophilicity are the structural features affecting this series cytotoxic activity. Molecular docking study for the most potent cytotoxic compounds (**7c** and **8a-c**) rationalized their superior CDK2 inhibitory activity through their hydrogen bonding interactions with the key amino acids in the ATP binding site (Leu83, Lys89 and Asp145) and through hydrophobic interaction with the hydrophobic side chains of the amino acids Ile10, Val18, Ala31, Val 64 and Phe 80 and Gln 85. This was reflected in their high docking score relative to the co-crystalized inhibitor RC-1-148 (−13.00 - −13.66 *vs* −11.11 kcal/mol). Finally, the promising pharmacokinetic properties of the most potent compounds were also proven indicating that the newly synthesized compounds are not only with promising antitumor activity but also possess promising pharmacokinetic properties. This all motivates us to introduce these compounds as potent and promising anticancer agents for further biological and pharmacological studies to pave their way successfully to the clinical studies.

5. Experimental

5.1. Chemistry

All melting points are uncorrected and were taken in open capillary tubes using Electrothermal apparatus 9100. Elemental microanalyses were carried out at Microanalytical Unit, Central Services Laboratory, National Research Centre, Dokki, Cairo, Egypt, using Vario Elementar and were found within ± 0.4% of the theoretical values. Infrared spectra were recorded on a FT/IR-4100 Jasco-Japan, Fourier transform, Infrared spectrometer at cm^{-1} scale using KBr disc technique at Central Services Laboratory, National Research Center, Dokki, Cairo, Egypt. ^1H NMR and ^{13}C NMR spectra were determined by using a Merury Plus-Oxford 400 MHZ at Ministry of defense, Chemical Warfare Department, The Main Chemical Warfare Laboratories, Cairo, Egypt and Bruker High Performance Digital FT-NMR Spectrometer Avance III 400 MHz, Faculty of Pharmacy-Cairo University, Cairo, Egypt. Chemical shifts were expressed in δ (ppm) downfield from TMS as an internal standard. Follow up of the reactions and checking the purity of the compounds were made by TLC on silica gel-precoated aluminum sheets (Type 60, F 254, Merck, Darmstadt, Germany) using chloroform/methanol (20:2, v/v) and the spots were detected by exposure to UV lamp at λ254 nm for few seconds and by iodine vapor. The chemical names given for the prepared compounds are according to the IUPAC system. 3-Acetyl-6-substituted-2*H*-chromen-2-one **1a-c** [38] and 2-(1-(6-substituted-2-Oxo-2*H*-chromen-3-yl)ethylidene)hydrazinecarbothioamide **2a-c** [37,38] was prepared according to the reported method.

5.1.1. General procedure for the synthesis of 3-(1-(2-(substituted thiazol-2-yl)hydrazono)ethyl)-6-substituted-2H-chromen-2-one 3a-c-8a-c and 2-(1-(6-substituted-2-oxo-2H-chromen-3-yl)ethylidene)hydrazono)thiazolidin-4-one 9a-c

To a hot solution of carbothioamide derivatives **2a-c** (0.005 mol) in absolute ethanol (15 mL), anhydrous sodium acetate (0.41 g, 0.005 mol) was added. To the previous mixture, each of, chloroacetone (0.46 g, 0.005 mol), phenacyl bromide (0.99 g, 0.005 mol), 4-bromophenacylbromide (1.39 g, 0.005 mol), 2-bromoacetyltetralin (1.33 g, 0.005 mol), 3-chloroacetylacetone (0.67 g, 0.005 mol), ethyl-2-chloroacetoacetate (0.82 mL, 0.005 mol) and ethyl bromoacetate (0.84 mL, 0.005 mol) was added and the reaction mixture was refluxed for 2–4 h. The progress of the reaction was monitored by TLC. The reaction mixture was allowed to cool, the formed precipitate was filtered, washed several times with water, dried, and recrystallized from ethanol to give the title compounds **3a-c**-**9a-c**.

5.1.2. 3-(1-(2-(4-Methylthiazol-2-yl)hydrazono)ethyl)-2H-chromen-2-one (3a)

Yield 67%, mp 128–129 °C, IR (ν_{max}/cm^{-1}): 3191 (NH), 3061 (CH-arom.), 2930, 2848 (CH-aliph.), 1718 (CO). ^1H NMR ($CDCl_3$): δ 2.31 (3H, s, CH_3), 2.35 (3H, s, CH_3), 6.25 (1H, s, Ar-H), 7.28–7.36 (2H, m, Ar-H), 7.54–7.61 (2H, m, Ar-H), 8.03 (1H, s, Ar-H), 8.78 (1H, s, NH, D_2O exchangeable). ^{13}C NMR ($CDCl_3$): δ 15.35, 16.70, 103.67, 116.49, 119.13, 124.68, 126.29, 128.69, 132.15, 141.15, 145.94, 146.43, 153.96, 159.90, 168.73. MS, *m/z* (%): $[M+2]^{+\cdot}$ 301 (89.44), $M^{+\cdot}$ 299 (11.05%).Anal. For $C_{15}H_{13}N_3O_2S$ (299.35): Calcd. C, 60.19; H, 4.38; N, 14.04; S, 10.71. Found: C, 60.23; H, 4.01; N, 14.32; S, 10.46.

5.1.3. 6-Chloro-3-(1-(2-(4-methylthiazol-2-yl)hydrazono)ethyl)-2H-chromen-2-one (3b)

Yield 78%, mp > 300 °C, IR (ν_{max}/cm^{-1}): 3220 (NH), 3060 (CH-arom.), 2926, 2861 (CH-aliph.), 1711 (CO).^1H NMR ($CDCl_3$): δ 2.30 (3H, s, CH_3), 2.72 (3H, s, CH_3), 7.28–7.63 (3H, m, Ar-H), 7.94 (1H, s, Ar-H), 8.40 (1H, s, Ar-H), 11.86 (1H, s, NH, D_2O exchangeable). ^{13}C NMR ($CDCl_3$): δ 14.09, 29.68, 117.91, 118.16, 127.75, 129.08, 130.32, 131.99, 134.23, 146.07, 154.01. MS, *m/z* (%): $M^{+\cdot}$ 333 (6.86%), $[M-2]^{+\cdot}$ 331 (9.91). Anal. For $C_{15}H_{12}ClN_3O_2S$ (333.79): Calcd. C,

53.97; H, 3.62; N, 12.59; S, 9.61. Found: C, 53.68; H, 3.41; N, 12.76; S, 9.41.

5.1.4. 6-Bromo-3-(1-(2-(4-methylthiazol-2-yl)hydrazono)ethyl)-2H-chromen-2-one (3c)

Yield 45%, mp 244–245 °C, IR (ν_{max}/cm^{-1}): 3159 (NH), 3053 (CH-arom.), 2926, 2867 (CH-aliph.), 1713 (CO). ^{1}H NMR ($CDCl_3$): δ 2.33 (3H, s, CH_3), 2.43 (3H, s, CH_3), 7.19–7.75 (3H, m, Ar-H), 7.91 (1H, s, Ar-H), 8.35 (1H, s, Ar-H), 12.07 (1H, s, NH, D_2O exchangeable). ^{13}C NMR ($CDCl_3$): δ 16.88, 29.60, 117.53, 118.26, 118.35, 119.64, 120.23, 125.26, 131.00, 132.21, 135.42, 137.10, 140.93, 146.19, 152.83. MS, *m/z* (%): $[M+2]^{+\cdot}$ 380 (89.44), $M^{+\cdot}$ 378 (11.05%).Anal. For $C_{15}H_{12}BrN_3O_2S$ (378.24): Calcd. C, 47.63; H, 3.20; N, 11.11; S, 8.48. Found: C, 47.28; H, 3.41; N, 11.33; S, 8.15.

5.1.5. 3-(1-(2-(4-Phenylthiazol-2-yl)hydrazono)ethyl)-2H-chromen-2-one (4a)

Yield 61%, mp 243–244 °C, IR (ν_{max}/cm^{-1}): 3184 (NH), 3060 (CH-arom.), 2932, 2841 (CH-aliph.), 1718 (CO). ^{1}H NMR ($CDCl_3$): δ 2.63 (3H, s, CH_3), 6.82 (1H, s, Ar-H), 7.33–7.77 (9H, m, Ar-H), 8.03 (1H, s, Ar-H), 13.04 (1H, br s, NH, D_2O exchangeable). ^{13}C NMR ($CDCl_3$): δ 17.84, 101.23, 116.75, 118.60, 124.92, 125.23, 125.70, 126.19, 128.21, 128.76, 128.82, 128.96, 129.70, 130.24, 130.66, 133.07, 142.54, 154.31, 155.34, 170.17. MS, *m/z* (%): $M^{+\cdot}$ 361 (30.09%).Anal. For$C_{20}H_{15}N_3O_2S$ (361.42): Calcd. C, 66.47; H, 4.18; N, 11.63; S, 8.87. Found: C, 66.21; H, 4.30; N, 11.74; S, 8.61.

5.1.6. 6-Chloro-3-(1-(2-(4-phenylthiazol-2-yl)hydrazono)ethyl)-2H-chromen-2-one (4b)

Yield 63%, mp 245–246 °C, IR (ν_{max}/cm^{-1}): 3229 (NH), 3032 (CH-arom.), 2913, 2820 (CH-aliph.), 1739 (CO). ^{1}H NMR ($CDCl_3$): δ 2.42 (3H, s, CH_3), 7.32–7.76 (8H, m, Ar-H), 7.88 (1H, s, Ar-H), 7.93 (1H, s, Ar-H), 12.53 (1H, s, NH, D_2O exchangeable). ^{13}C NMR ($CDCl_3$): δ 23.08, 100.99, 118.16, 118.33, 119.14, 125.64, 125.70, 127.99, 128.66, 129.61, 129.72, 130.51, 130.71, 133.37, 140.09, 143.54, 146.02, 152.04. MS, *m/z* (%): $[M+2]^{+\cdot}$ 397 (12.09), $M^{+\cdot}$ 395 (38.18%). Anal. For $C_{20}H_{14}ClN_3O_2S$ (395.86): Calcd. C, 60.68; H, 3.56; N, 10.61; S, 8.10. Found: C, 60.91; H, 3.23; N, 10.38; S, 7.84.

5.1.7. 6-Bromo-3-(1-(2-(4-phenylthiazol-2-yl)hydrazono)ethyl)-2H-chromen-2-one (4c)

Yield 75%, mp 244–245 °C, IR (ν_{max}/cm^{-1}): 3226 (NH), 3050 (CH-arom.), 2926, 2864 (CH-aliph.), 1726 (CO). ^{1}H NMR ($CDCl_3$): δ 2.44 (3H, s, CH_3), 7.21–7.79 (8H, m, Ar-H), 7.96 (1H, s, Ar-H), 8.37 (1H, s, Ar-H), 11.74 (1H, s, NH, D_2O exchangeable). ^{13}C NMR ($CDCl_3$): δ 20.54, 121.37, 122.18, 122.29, 124.27, 129.78, 130.02, 130.49, 132.67, 132.93, 133.12, 133.53, 133.75, 134.97, 139.32, 144.85, 156.73, 163.03. MS, *m/z* (%): $[M+1]^{+\cdot}$ 441 (16.79), $[M-1]^{+\cdot}$ 439 (8.54%). Anal. For $C_{20}H_{14}BrN_3O_2S$ (440.31): Calcd. C, 54.56; H, 3.20; N, 9.54; S, 7.28. Found: C, 54.71; H, 3.43; N, 9.22; S, 7.45.

5.1.8. 3-(1-(2-(4-(4-Bromophenyl)thiazol-2-yl)hydrazono)ethyl)-2H-chromen-2-one (5a)

Yield 79%, mp 230–231 °C, IR (ν_{max}/cm^{-1}): 3229 (NH), 3032 (CH-arom.), 2943, 2828 (CH-aliph.), 1739 (CO). ^{1}H NMR ($CDCl_3$): δ 2.63 (3H, s, CH_3), 6.83 (1H, s, Ar-H), 7.15–7.94 (8H, m,Ar-H), 8.03 (1H, s, Ar-H), 12.96 (1H, br s, NH, D_2O exchangeable). MS, *m/z* (%): $[M+2]^{+\cdot}$ 442 (16.83), $M^{+\cdot}$ 440 (18.07%). Anal. For $C_{20}H_{14}BrN_3O_2S$ (440.31): Calcd. C, 54.56; H, 3.20; N, 9.54; S, 7.28.Found: C, 54.36; H, 3.18; N, 9.66; S, 7.01.

5.1.9. 3-(1-(2-(4-(4-Bromophenyl)thiazol-2-yl)hydrazono)ethyl)-6-chloro-2H-chromen-2-one (5b)

Yield 72%, mp 271–272 °C, IR (ν_{max}/cm^{-1}): 3315 (NH), 3061 (CH-arom.), 2928, 2851 (CH-aliph.), 1718 (CO). ^{1}H NMR ($CDCl_3$): δ 2.63 (3H, s, CH_3), 6.84 (1H, s, Ar-H), 7.25–7.91 (7H, m, Ar-H), 7.95 (1H, s, Ar-H), 12.98 (1H, br s, NH, D_2O exchangeable). MS, *m/z* (%): $[M+2]^{+\cdot}$ 476 (16.07), $M^{+\cdot}$ 474 (49.07%). Anal. For$C_{20}H_{13}BrClN_3O_2S$ (474.76): Calcd. C, 50.60; H, 2.76; N, 8.85; S, 6.75. Found: C, 50.72; H, 2.51; N, 8.62; S, 6.48.

5.1.10. 6-Bromo-3-(1-(2-(4-(4-bromophenyl)thiazol-2-yl)hydrazono) ethyl)-2H-chromen-2-one (5c)

Yield 66%, mp 239–240 °C, IR (ν_{max}/cm^{-1}): 3111 (NH), 3059 (CH-arom.), 2928, 2864 (CH-aliph.), 1718 (CO). ^{1}H NMR ($CDCl_3$): δ 2.63 (3H, s, CH_3), 6.84 (1H, s, Ar-H), 7.28–7.80 (6H, m, Ar-H), 7.95 (1H, s, Ar-H), 8.42 (1H, s, Ar-H), 13.00 (1H, br s, NH, D_2O exchangeable). ^{13}C NMR ($CDCl_3$): δ 29.58, 118.28, 120.18, 126.34, 127.31, 131.02, 132.51, 135.53, 137.10, 141.00, 148.01, 150.11. MS, *m/z* (%): $M^{+\cdot}$ 519 (1.22%), $[M-2]^{+\cdot}$ 517 (2.26). Anal. For $C_{20}H_{13}Br_2N_3O_2S$ (519.21): Calcd. C, 46.27; H, 2.52; N, 8.09; S, 6.18. Found: C, 46.09; H, 2.61; N, 8.23; S, 6.30.

5.1.11. 3-(1-(2-(4-(5,6,7,8-Tetrahydronaphthalen-2-yl)thiazol-2-yl) hydrazono)ethyl)-2H-chromen-2-one (6a)

Yield 78%, mp226-227 °C, IR (ν_{max}/cm^{-1}): 3393 (NH), 3064 (CH-arom.), 2925, 2856 (CH-aliph.), 1721 (CO). ^{1}H NMR ($CDCl_3$): δ 1.77–1.82 (4H, m, 2(CH_2)-tetrahydronaphthalene protons), 2.57 (3H, s, CH_3), 2.78–2.83 (4H, m, 2(CH_2)-tetrahydronaphthaleneprotons), 6.70 (1H, s, Ar-H), 7.14 (1, d, Ar-H, J = 8.00 Hz), 7.33–7.62(6H, m, Ar-H), 8.01 (1H, s, Ar-H), 12.47 (1H, s, NH, D_2O exchangeable). ^{13}C NMR ($CDCl_3$): δ 16.63, 22.85, 29.34, 29.41, 100.26, 116.70, 118.67, 12.75, 124.88, 125.34, 126.33, 128.94, 130.31, 132.94, 138.60, 140.23, 142.29, 142.37, 154.26, 159.08, 169.92. MS, *m/z* (%): $M^{+\cdot}$ 415 (33.07%). Anal. For $C_{24}H_{21}N_3O_2S$ (415.51): Calcd. C, 69.37; H, 5.09; N, 10.11; S, 7.72. Found: C, 69.25; H, 5.31; N, 10.28; S, 7.60.

5.1.12. 6-Chloro-3-(1-(2-(4-(5,6,7,8-tetrahydronaphthalen-2-yl)thiazol-2-yl)hydrazono)ethyl)-2H-chromen-2-one (6b)

Yield 65%, mp 259–260 °C, IR (ν_{max}/cm^{-1}): 3125 (NH), 3054 (CH-arom.), 2927, 2863 (CH-aliph.), 1720 (CO). ^{1}H NMR ($CDCl_3$): δ 1.68–1.72 (4H, m,2(CH_2)-tetrahydronaphthalene protons), 2.51 (3H, s, CH_3), 2.69–2.75 (4H, m, 2(CH_2)-tetrahydronaphthalene protons), 6.65–8.01 (8H, m, Ar-H), 12.62 (1H, s, NH, D_2O exchangeable). MS, *m/z* (%): $[M+2]^{+\cdot}$ 452 (10.03), $M^{+\cdot}$ 450 (33.15%).Anal. For$C_{24}H_{20}ClN_3O_2S$ (449.95): Calcd. C, 64.06; H, 4.48; N, 9.34; S, 7.13. Found: C, 64.24; H, 4.31; N, 9.22; S, 7.29.

5.1.13. 6-Bromo-3-(1-(2-(4-(5,6,7,8-tetrahydronaphthalen-2-yl)thiazol-2-yl)hydrazono)ethyl)-2H-chromen-2-one (6c)

Yield 70%, mp 262–263 °C, IR (ν_{max}/cm^{-1}): 3169 (NH), 3053 (CH-arom.), 2925, 2858 (CH-aliph.), 1730 (CO). ^{1}H NMR ($CDCl_3$): δ 1.68–1.74 (4H, m, 2(CH_2)-tetrahydronaphthalene protons), 2.49 (3H, s, CH_3), 2.71–2.75 (4H, m, 2(CH_2)-tetrahydronaphthalene protons), 7.08–7.71 (7H, m, Ar-H), 7.91 (1H, s, Ar-H), 11.85 (1H, s, NH, D_2O exchangeable). ^{13}C NMR ($CDCl_3$): δ 17.39, 22.73, 29.25, 29.57, 117.43, 118.29, 120.12, 122.75, 126.37, 130.14, 131.05, 135.58, 138.48, 140.13, 141.20, 152.87, 158.69. MS, *m/z* (%): $[M+2]^{+\cdot}$ 496 (13.59), $M^{+\cdot}$ 494 (15.84%). Anal. For $C_{24}H_{20}BrN_3O_2S$ (494.40): Calcd. C, 58.30; H, 4.08; N, 8.50; S, 6.49. Found: C, 58.01; H, 4.27; N, 8.37; S, 6.54.

5.1.14. 3-(1-(2-(5-Acetyl-4-methylthiazol-2-yl)hydrazono)ethyl)-2H-chromen-2-one (7a)

Yield 57%, mp 198–199 °C, IR (ν_{max}/cm^{-1}): 3179 (NH), 3086 (CH-arom.), 2924, 2854 (CH-aliph.), 1724, 1710 (2CO). ^{1}H NMR ($CDCl_3$): δ 2.38 (3H, s, CH_3), 2.61 (3H, s, CH_3), 2.71 (3H, s, CH_3), 7.23–7.77 (3H, m, Ar-H), 7.96 (1H, s, Ar-H), 8.39 (1H, s, Ar-H), 13.02 (1H, s, NH, D_2O exchangeable). ^{13}C NMR ($CDCl_3$): δ 15.74, 16.33, 30.50, 117.37, 118.40, 120.41, 125.41, 126.73, 131.00, 132.17, 135.21, 137.01, 140.28, 145.96, 154.06, 158.53, 195.02. MS, *m/z* (%): $M^{+\cdot}$ 341 (22.18%). Anal. For $C_{17}H_{15}N_3O_3S$ (341.38): Calcd. C, 59.81; H, 4.43; N, 12.31; S, 9.39. Found: C, 59.63; H, 4.26; N, 12.09; S, 9.17.

5.1.15. 3-(1-(2-(5-Acetyl-4-methylthiazol-2-yl)hydrazono)ethyl)-6-chloro-2H-chromen-2-one (7b)

Yield 61%, mp 227–228 °C, IR (ν_{max}/cm^{-1}): 3256 (NH), 3049 (CH-arom.), 2925, 2857 (CH-aliph.), 1721 (CO). ^{1}H NMR ($CDCl_3$): δ 2.29 (3H, s, CH_3), 2.39 (3H, s, CH_3), 2.52 (3H, s, CH_3), 7.23–7.59 (3H, m, Ar-H), 7.94 (1H, s, Ar-H), 13.00 (1H, s, NH, D_2O exchangeable). ^{13}C NMR ($CDCl_3$): δ 15.53, 17.78, 29.70, 117.85, 118.09, 120.05, 127.07, 127.89, 129.11, 130.07, 132.23, 134.31, 140.38, 146.33, 152.21, 159.48, 190.28. MS, *m/z* (%): $[M+2]^{+\cdot}$ 378 (8.91), $M^{+\cdot}$ 376 (23.04%). Anal. For $C_{17}H_{14}ClN_3O_3S$ (375.83): Calcd. C, 54.33; H, 3.75; N, 11.18; S, 8.53. Found: C, 54.12; H, 3.45; N, 11.29; S, 8.72.

5.1.16. 3-(1-(2-(5-Acetyl-4-methylthiazol-2-yl)hydrazono)ethyl)-6-bromo-2H-chromen-2-one (7c)

Yield 55%, mp 204–205 °C, IR (ν_{max}/cm^{-1}): 3291 (NH), 3053 (CH-arom.), 2926, 2868 (CH-aliph.), 1726 (CO). ^{1}H NMR ($CDCl_3$): δ 2.30 (3H, s, CH_3), 2.41 (3H, s, CH_3), 2.54 (3H, s, CH_3), 7.18–7.75 (2H, m, Ar-H), 7.95 (1H, s, Ar-H), 8.36 (1H, s, Ar-H), 12.86 (1H, s, NH, D_2O exchangeable). ^{13}C NMR ($CDCl_3$): δ 15.46, 17.94, 29.56, 117.35, 117.53, 118.35, 120.53, 127.07, 130.95, 132.21, 135.02, 137.10, 140.19, 146.19, 152.69, 159.40, 190.23. MS, *m/z* (%): $[M+2]^{+\cdot}$ 422 (16.07), $M^{+\cdot}$ 420 (45.09%).Anal. For$C_{17}H_{14}BrN_3O_3S$ (420.28): Calcd.C, 48.58; H, 3.36; N, 10.00; S, 7.63.Found: C, 48.39; H, 3.42; N, 10.23; S, 7.51.

5.1.17. Ethyl 4-methyl-2-(2-(1-(2-oxo-2H-chromen-3-yl)ethylidene) hydrazinyl)thiazole-5-carboxylate (8a)

Yield 53%, mp 219–220 °C, IR (ν_{max}/cm^{-1}): 3225 (NH), 3082 (CH-arom.), 2936, 2858 (CH-aliph.), 1724 (CO). ^{1}H NMR ($CDCl_3$): δ1.37 (3H, t, $CO_2CH_2\mathbf{CH_3}$, J = 14.20), 2.38 (3H, s, CH_3), 2.63 (3H, s, CH_3), 4.34 (2H, q, $CO_2\mathbf{CH_2}CH_3$, J = 21.28), 7.28–7.39 (2H, m, Ar-H), 7.58–7.65 (2H, m, Ar-H), 8.08 (1H, s, Ar-H), 12.47 (1H, s, NH, D_2O exchangeable). ^{13}C NMR ($CDCl_3$): δ 14.81, 17.00, 26.86, 61.34, 116.48, 119.39, 125.25, 126.85, 129.79, 132.86, 141.58, 153.88, 157.00, 159.59, 162.37. MS, *m/z* (%): $M^{+\cdot}$ 371 (32.63%). Anal. For $C_{18}H_{17}N_3O_4S$ (371.41): Calcd. C, 58.21; H, 4.61; N, 11.31; S, 8.63.Found: C, 58.36; H, 4.50; N, 11.46; S, 8.81.

5.1.18. Ethyl 2-(2-(1-(6-chloro-2-oxo-2H-chromen-3-yl)ethylidene) hydrazinyl)-4-methylthiazole-5-carboxylate (8b)

Yield 61%, mp 189–190 °C, IR (ν_{max}/cm^{-1}): 3256 (NH), 3048 (CH-arom.), 2978, 2851 (CH-aliph.), 1724 (CO). ^{1}H NMR ($CDCl_3$): δ1.35 (3H, t, $CO_2CH_2\mathbf{CH_3}$, J = 14.40), 2.34 (3H, s, CH_3), 2.72 (3H, s, CH_3), 4.31 (2H, q, $CO_2\mathbf{CH_2}CH_3$, J = 21.80), 7.29–7.63 (2H, m, Ar-H), 7.99 (1H, s, Ar-H), 8.40 (1H, s, Ar-H), 12.69 (1H, s, NH, D_2O exchangeable). ^{13}C NMR ($CDCl_3$): δ 14.40, 14.97, 17.20, 60.80, 117.94, 118.16, 120.05, 127.89, 129.08, 130.07, 130.31, 132.23, 132.57, 134.23, 140.11, 146.06, 152.34, 169.0. MS, *m/z* (%): $M^{+\cdot}$ 406 (3.92%), $[M-2]^{+\cdot}$ 404 (9.92). Anal. For $C_{18}H_{16}ClN_3O_4S$ (405.86): Calcd. C, 53.27; H, 3.97; N, 10.35; S, 7.90.Found: C, 53.42; H, 3.81; N, 10.16; S, 7.72.

5.1.19. Ethyl 2-(2-(1-(6-bromo-2-oxo-2H-chromen-3-yl)ethylidene) hydrazinyl)-4-methylthiazole-5-carboxylate (8c)

Yield 66%, mp 181–182 °C, IR (ν_{max}/cm^{-1}): 3221 (NH), 3044 (CH-arom.), 2924, 2851 (CH-aliph.), 1732 (CO). ^{1}H NMR ($CDCl_3$): δ1.39 (3H, t, $CO_2CH_2\mathbf{CH_3}$, J = 13.96), 2.50 (3H, s, CH_3), 2.70 (3H, s, CH_3), 4.37 (2H, q, $CO_2\mathbf{CH_2}CH_3$, J = 21.08), 7.28 (1H, s, Ar-H), 7.68–7.99 (2H, m, Ar-H), 8.42 (1H, s, Ar-H), 12.53 (1H, s, NH, D_2O exchangeable). ^{13}C NMR ($CDCl_3$): δ 14.31, 15.36, 16.64, 61.77, 117.53, 118.43, 119.73, 120.25, 125.44, 126.47, 131.09, 132.19, 135.52, 137.04, 140.75, 145.98, 154.09, 169.10. MS, *m/z* (%): $[M+2]^{+\cdot}$ 452 (12.83), $M^{+\cdot}$ 450 (15.08%). Anal. For $C_{18}H_{16}BrN_3O_4S$ (450.31): Calcd. C, 48.01; H, 3.58; N, 9.33; S, 7.12. Found: C, 48.27; H, 3.32; N, 9.14; S, 6.86.

5.1.20. 2-((1-(2-Oxo-2H-chromen-3-yl)ethylidene)hydrazono)thiazolidin-4-one (9a)

Yield 56%, mp 241–242 °C, IR (ν_{max}/cm^{-1}): 3101 (NH), 3066 (CH-arom.), 2970, 2846 (CH-aliph.), 1738, 1709 (CO). ^{1}H NMR ($CDCl_3$): δ 2.64 (3H, s, CH_3), 3.89 (2H, s, CH_2), 7.34–7.63 (4H, m, Ar-H), 8.10 (1H, s, Ar-H), 11.40 (1H, br s, NH, D_2O exchangeable). ^{13}C NMR ($CDCl_3$): δ 17.19, 32.88, 116.52, 124.61, 128.84, 132.40, 141.95, 152.01, 168.03. MS, *m/z* (%): $M^{+\cdot}$ 301 (17.72%). Anal. For $C_{14}H_{11}N_3O_3S$ (301.32): Calcd. C, 55.80; H, 3.68; N, 13.95; S, 10.64. Found: C, 55.62; H, 3.51; N, 13.80; S, 10.43.

5.1.21. 2-((1-(6-Chloro-2-oxo-2H-chromen-3-yl)ethylidene)hydrazono) thiazolidin-4-one (9b)

Yield 50%, mp 252–253 °C, IR (ν_{max}/cm^{-1}): 3198 (NH), 3066 (CH-arom.), 2970, 2847 (CH-aliph.), 1735, 1708 (CO). ^{1}H NMR ($CDCl_3$): δ 2.74 (3H, s, CH_3), 3.91 (2H, s, CH_2), 7.65–8.04 (3H, m, Ar-H), 8.42 (1H, s, Ar-H), 11.60 (1H, s, NH, D_2O exchangeable). MS, *m/z* (%): $[M+2]^{+\cdot}$ 338 (13.28), $M^{+\cdot}$ 336 (38.03%). Anal. For $C_{14}H_{10}ClN_3O_3S$ (335.77): Calcd. C, 50.08; H, 3.00; N, 12.51; S, 9.55. Found: C, 50.25; H, 3.22; N, 12.28; S, 9.36.

5.1.22. 2-((1-(6-Bromo-2-oxo-2H-chromen-3-yl)ethylidene)hydrazono) thiazolidin-4-one (9c)

Yield 52%, mp 258–259 °C, IR (ν_{max}/cm^{-1}): 3150 (NH), 3065 (CH-arom.), 2916, 2847 (CH-aliph.), 1732 (CO). ^{1}H NMR ($CDCl_3$): δ 2.72 (3H, s, CH_3), 3.48 (2H, s, CH_2), 6.99–8.01 (3H, m, Ar-H), 8.41 (1H, s, Ar-H), 11.49 (1H, s, NH, D_2O exchangeable). MS, *m/z* (%): $[M+2]^{+\cdot}$ 382 (12.05), $M^{+\cdot}$ 380 (16.48%). Anal. For $C_{14}H_{10}BrN_3O_3S$ (380.22): Calcd. C, 44.22; H, 2.65; N, 11.05; S, 8.43. Found: C, 44.03; H, 2.42; N, 11.23; S, 8.52.

5.2. Biological Screening

5.2.1. In- vitro anticancer activity

The *in vitro* cytotoxicity of the newly synthesized compounds against HeLa cancer cell line was performed with the MTT assay [76]. The MTT assay is based on the reduction of the soluble 3-(4,5-methyl-2-thiazolyl)-2,5-diphenyl-2H-tetrazolium bromide (MTT) into a blue-purple formazan product, mainly by mitochondrial reductase activity inside living cells. The cells used in cytotoxicity assay were cultured in RPMI 1640 medium supplemented with 10% fetal calf serum. Cells suspended in the medium (2×10^4/mL) were plated in 96-well culture plates and incubated at 37 °C in a 5% CO_2 incubator. After 12 h, the test sample (2 µl) was added to the cells (2×10^4) in 96-well plates and cultured at 37 °C for 3 days.

The cultured cells were mixed with 20 µl of MTT solution and incubated for 4 h at 37 °C. The supernatant was carefully removed from each well and 100 µl of DMSO were added to each well to dissolve the formazan crystals which were formed by the cellular reduction of MTT. After mixing with a mechanical plate mixer, the absorbance of each well was measured by a microplate reader using a test wavelength of 570 nm.

The results were expressed as the IC_{50} (µM), inducing a 50% inhibition of cell growth of treated cells when compared to the growth of control cells. Each experiment was performed at least 3 times. There was a good reproducibility between replicate wells with standard errors reported in Table 1.

5.2.2. Cell cycle analysis and apoptosis detection

Cell cycle analysis and apoptosis detection were carried out by flow cytometry [77]. HeLa cells were seeded at 8×10^4 and incubated at 37 °C, in 5% CO_2 incubator overnight, after 24 h from treatment with the tested compound, cell pellets were collected and centrifuged ($300 \times$ g, for 5 min). For cell cycle analysis, cell pellets were fixed with 70% ethanol on ice for 15 min and collected again. The collected pellets were incubated with propidium iodide (PI) staining solution (50 µg/mL

PI, 0.1 mg/mL RNaseA, 0,05% Triton X-100) at room temperature for 1 h. and analyzed by Gallios flow cytometer (Beckman Coulter, Brea, CA, USA).

Apoptosis detection was performed by FITC Annexin-V/PI commercial kit (Becton Dickenson, Franklin Lakes, NJ, USA) following the manufacture protocol. The samples were analyzed by fluorescence-activated cell sorting (FACS) with a Gallios flow cytometer (Beckman Coulter, Brea, CA, USA) within 1 h after staining. Data were analyzed using Kaluzav1.2 (Beckman Coulter).

5.2.3. CDK2/ E1 enzyme assay

ADP-Glo™ Kinase Assay is a luminescent kinase assay that measures ADP formed from a kinase reaction; ADP is converted into ATP, which is converted into light by Ultra-Glo™ Luciferase. The luminescent signal positively correlates with ADP amount and kinase activity. The assay was performed according to the protocol supplied from CDK2/CyclinE1 Kinase Assay kit, Promegra Cat. # V4488., along with the following steps: 1stDilute enzyme, substrate, ATP and inhibitors in Kinase Buffer. Then add to the wells of 384 low volume plate: (a) 1 µl of inhibitor or (5% DMSO). (b) 2 µl of enzyme. (c) 2 µl of substrate/ATP mix. Then incubate at room temperature for 60 min. After that add 5 µl of ADP-Glo™ Reagent and the plate was incubated at room temperature for 40 min. Then add 10 µl of kinase detection reagent and incubate at room temperature for 30 min. Finally, the luminescence (Integration time 0.5–1 s) was recorded using bioline elisa reader at wave length 450 nm for each concentration of the analyzed compounds (0.01–10 ng/mL). The activity of the analyzed enzyme in the samples is then determined by comparing the % inhibition of the samples to the log conc. The concentration of the test compounds required to reduce the kinase activity by 50% was determined from dose-response curves and recorded as their IC50.

5.2.4. RT-PCR gene expression of P21 and P27

The RNA extraction and reverse transcription were performed using RNeasy micro kit (Quiagen-Germany-Cat.no 74004). While the PCR-RT assay was carried out using iScript TM One-Step RT-PCR Kit with SYBR® Greenkit (BioRad-USA - cat.no #345-0412) following the supplied protocol using (Rotorgene.S. Korea) PCR system reader. The isolated primers are as the following:

p21 F 5TGGAGACTCTCAGGGTCGAAA-3′ R 5′-CGGCGTTTGGAGTGGTAGAA-3′	p27 F 5′-CCGGTGGACCACGAAG AGT-3′ R 5′ -GCTCGCCTCTTCCATGTCTC-3′
CDK2 F 5′-GCTAGCAGACTTTGGACTAGC CAG-3′ R 5′-AGCTCGGTACCACAGGGTCA-3′	β-actin F 5′-GTGACATCCACACCCA GAGG-3′ β-actin R 5′-ACAGGATGTCAAAACT GCCC-3′

CT values of the target gene and housekeeping gene of both control cells and treated cells are used to calculate the fold change and hence the results could be interpreted.

5.2.5. Caspases -9 and caspase-3 assays

Activities of caspase -9 and caspase -3 were measured using DRG® Caspase-9 (human) ELISA (EIA-4860) *kit (DRG International Inc., USA), Invitrogen* Caspase-*3 (Active)* (human) ELISA *kit, Catalog # KHO1091 (96 tests)(Invitrogen Corporation, USA)* according to the manufacturer instruction. Briefly, HeLa cells were treated with IC_{50} concentration of compound **8a**. The cells were harvested by trypsinization and rinsed with PBS. After centrifugation, the pellet (105–106 cells) was suspended in 1 mL of PBS. Cells were frozen at < -20 °C and thawed with gentle mixing. Freeze/thaw cycle repeated for 3 times, then centrifuged at 1500*g* for 10 min. at 2–8 °C to remove cellular debris. Human ELISA kit is a solid phase sandwich (ELISA). A monoclonal specific antibody for human target protein has been coated onto the wells of the microtiter strips provided. Samples, including a standard containing the human target protein control specimens, and unknowns, are pipetted into these wells and then a rabbit antibody specific for human active target protein is added to the wells. During the first incubation, the human target protein binds to the immobilized (capture) antibody and the specific active protein antibody serves as a detection antibody by binding to the immobilized active protein. After the first incubation step and washing to remove excess protein and detection antibody, a horseradish peroxidase-labeled AntiRabbit IgG (Anti-Rabbit IgG HRP) is added. This binds to the detection antibody to complete the four-member sandwich. After a third incubation and washing to remove all the excess AntiRabbit IgG HRP, a substrate solution is added, which is acted upon by the bound enzyme to produce color. The color intensity is measured using ROBONIK P2000 SPECTROPHOTOMETER at a wavelength of 450 nm. The intensity of this colored product is directly proportional to the concentration of human active protein present in the original specimen [78].

5.3. Molecular modeling studies:

QSAR and molecular docking studies were carried out using Molecular Operating Environment (MOE, 10.2008) software. All structure minimizations were performed with MOE until an RMSD gradient of 0.1 kcal·mol^{-1}Å^{-1} with MMFF94x force field and the partial charges were automatically calculated.

5.3.1. QSAR study

5.3.1.1. Drawing structures and molecular descriptors calculation. Compounds 3D structures were built using MOE software. The built compounds were then energy minimized. Finally, MOE molecular mechanical descriptors were calculated for all compounds resulting in a descriptor pool of 313 descriptors.

5.3.1.2. Training set and test set generation. The 16 newly synthesized compounds were split into a training set of 13 molecules and an external validation test set of 3 molecules such that the test set maintains the activity value distribution of the original dataset. Training and test set were then saved as “comma-separated values” files (.csv).

5.3.1.3. QSAR model generation and validation. It is worth mention here that model generation was performed using the training set only, while the test set was kept aside. RapidMiner 7.1.000 Basic Edition [52–54] was first used to remove the redundant descriptors which showed low variance among the different compounds using “*Remove Useless Attributes*“ operator as they add no additional information to the model, this left a set of 286 descriptors.

The descriptors remained after this initial filtration were used to generate the QSAR model. Forward selection algorithm (FSA) implemented in RapidMiner 7.1.000 Basic Edition was used to select the descriptors that are most relevant to the biological activity. Multiple Linear Regression (MLR) implemented in RapidMiner was used as the machine learning algorithm for linear model generation which removes co-linear descriptors by default. In FSA, Leave-one-out (LOO) cross-validation root-mean-square error ($RMSE_{CV}$) was used to assess the model performance for the selection of the best model during descriptor selection.

In addition to LOO cross-validation used for model internal validation, an external validation was performed by the application of the obtained model on the independent test set to assess the model predictive ability of unseen data points which is the actual measure for the model robustness.

5.3.2. Molecular docking study

The X-ray crystallographic structure of CDK2 enzyme co-crystallized with the diaminothiazole derivative RC-1-148 as inhibitor (PDB ID: 3QTR) was downloaded from the protein data bank. [63,79] All water

molecules were removed except one molecule involved in the co-crystalized ligand binding (Fig. 2). The protein structure was prepared for docking study using *Protonate 3D* protocol in MOE with default options. The co-crystalized ligand (RC-1-148) was used to define the active site for the docking algorithm. Triangle Matcher placement method and London dG scoring function were used to perform docking and scoring.

Docking protocol was first validated by re-docking of the co-crystallized ligand (RC-1-148) in the vicinity of the enzyme active site giving energy score (S) = −11.11 kcal/mol and RMSD of 0.509 Å (Fig. 2). The validated docking protocol was then used to study the ligand-target interactions in the active site for the most potent newly synthesized compounds **7c** and **8a-c** to predict their binding mode to rationalize their promising activity and to understand their structure activity relationship (SAR). The detailed description of the docking methodology is provided in supplementary data

5.3.3. Physicochemical, ADME and pharmacokinetic properties prediction

The free *Swiss ADME* web tool available from the Swiss Institute of Bioinformatics (SIB) was used for the calculation of the physicochemical descriptors as well as to predict the ADME parameters, pharmacokinetic properties, drug like nature and medicinal chemistry friendliness of the most potent newly synthesized compounds **7c** and **8a-c** [64,66,67,80]. The compounds' structures were converted to SMILES notations, then submitted to the online server for calculation.

Acknowledgments

The authors extend their appreciation and thanking to Dr. Essam Rashwan, head of confirmatory diagnostic unit, Vacsera-Egypt, for helping in performing the pharmacological screening.

This research article was funded by National Research Centre, Cairo, Egypt (2015-2016) through the project No. P100207 entitled "Synthesis and anticancer evaluation of novel thiazole-heterocyclic compounds". Consequently, the authors introduce their appreciation to the spirit of prof. Dr. Magdy I. El-Zahar, the first head of the project.

Conflict of interest

The authors have declared no conflict of interest.

Appendix A. Supplementary material

Supplementary data to this article can be found online at https://doi.org/10.1016/j.bioorg.2019.01.026.

References

[1] F.A.M. Al-Omary, G.S. Hassan, S.M. El-Messery, H.I. El-Subbagh, Synthesis and antitumor activity of novel thiazolo[2,3-b] quinazoline and pyrido[4,3-d]thiazolo [3,2-a]pyrimidine analogues, Eur. J. Med. Chem. 47 (2012) 65–72.
[2] F.Q. Alenzi, Limks between apoptosis, proliferation and the cell cycle, Br. J. Biomed Sci. 61 (2004) 99–102.
[3] B. Ouyang, J.A. Knauf, E.P. Smith, L. Zhang, T. Ramsey, N. Yusuff, D. Batt, J.A. Faqin, Inhibitors of Raf kinase activity block growth of thyroid cancer cells with RET/PTC or BRAF mutations in vitro and in vivo, Clin. Cancer. Res. 12 (2006) 1785–1793.
[4] J.A. McCubrey, L.S. Steelman, S.L. Abrams, W.H. Chappell, S. Russo, R. Ove, M. Milella, A. Tafuri, P. Lunghi, A. Bonati, F. Stivala, F. Nicoletti, M. Libra, A.M. Martelli, G. Montalto, M. Cervello, Emerging RAF inhibitors, Expert Opin. Emerg. Drugs. 14 (2009) 633–648.
[5] S. Lim, P. Kaldis, Cdks, cyclins and CKIs: roles beyond cell cycle regulation, Development. 140 (2013) 3079–3093.
[6] M. Malumbres, M. Barbacid, Mammalian cyclin-dependent kinases, Trends Biochem. Sci. 30 (2005) 630–641.
[7] S. Lapenna, A. Giordano, Cell cycle kinases as therapeutic targets for cancer, Nat. Rev. Drug Discovery. 8 (2009) 547–566.
[8] K.C. Luk, M.E. Simcox, A. Schutt, K. Rowan, T. Thompson, Y. Chen, U. Kammlott, W. DePinto, P. Dunten, A. Dermatakis, A new series of potent oxindole inhibitors of CDK2, Bioorg. Med. Chem. Lett. 14 (2004) 913–917.
[9] S. Cherukupalli, B. Chandrasekaran, V. Krystof, R.R. Aleti, N. Sayyad, S.R. Marugu, N.D. Kushwaha, R. Karpoormath, Synthesis, anticancer evaluation, and molecular docking studies of some novel 4,6-disubstituted pyrazolo[3,4-d]pyrimidines as cyclin dependent kinase 2 (CDK2) inhibitors, Bioorg. Chem. 79 (2018) 46–59.
[10] U. Asghar, A.K. Witkiewicz, N.C. Turner, E.S. Knudsen, The history and future of targeting cyclin dependent kinases in cancer therapy, Nat. Rev. Drug Discov. 14 (2015) 130–146.
[11] O. Tetsu, F. McCormick, Proliferation of cancer cells despite CDK2 inhibition, Cancer Cell 3 (2003) 233–245.
[12] T.A. Chohan, H. Qian, Y. Pan, J.Z. Chen, Cyclin-dependent kinase-2 as a target for cancer therapy: progress in the development of CDK2 inhibitors as anti-cancer agents, Curr. Med. Chem. 22 (2015) 237–263.
[13] D. Horiuchi, N.E. Huskey, L. Kusdra, L. Wohlbold, K.A. Merrick, C. Zhang, K.J. Creasman, K.M. Shokat, R.P. Fisher, A. Goga, Chemical-genetic analysis of cyclin dependent kinase 2 function reveals an important role in cellular transformation by multiple oncogenic pathways, Proc. Natl. Acad. Sci. U. S. A. 109 (2012) 1019–1027.
[14] S.J. Kashyap, V.K. Garg, P.K. Sharma, N. Kumar, R. Dudhe, J.K. Gupta, Thiazoles: having diverse biological activities, Med. Chem. Res. 21 (2012) 2123–2132.
[15] E. Gulsory, N.U. Guzeldemirci, Synthesis and primary cytotoxicity evaluation of new imidazo [2,1-b] thiazole derivatives, Eur. J. Med. Chem. 42 (2007) 320–326.
[16] M. Popsavin, S. Spaic, A. Svircev, V. Kojic, G. Bogdanovic, G. Popsavin, 2-(3-Amino-3-deoxy-b-D-xylofuranosyl)thiazole-4-carboxamide: a new tiazofurin analogue with potent antitumour activity, Bioorg. Med. Chem. 16 (2006) 5317–5320.
[17] R.M. Borzilleri, R.S. Bhide, J.C. Barrish, C.J. D'Arienzo, G.M. Derbin, J. Fargnoli, J.T. Hunt, R.Sr Jeyaseelan, A. Kamath, D.W. Kukral, P. Marathe, S. Mortillo, L. Qian, J.S. Tokarski, B.S. Wautlet, X. Zheng, L.J. Lombardo, Discovery and evaluation of N-cyclopropyl- 2,4-difluoro-5-((2-(pyridin-2-ylamino)thiazol-5-ylmethyl) amino)benzamide (BMS-605541), a selective and orally efficacious inhibitor of vascular endothelial growth factor receptor-2, J. Med. Chem. 49 (2006) 3766–3769.
[18] J. Wityak, J. Das, R.V. Moquin, Z. Shen, J. Lin, P. Chen, A.M. Doweyko, S. Pitt, S. Pang, D.R. Shen, Q. Fang, H.F. De Fex, G.L. Schieven, S.B. Kanner, J.C. Barrish, Discovery and initial SAR of 2-amino-5-carboxamidothiazoles as inhibitors of the Src-family kinase p56lck, Bioorg. Med. Chem. Lett. 13 (2003) 4007–4010.
[19] K.S. Kim, D. Kimball, R.N. Misra, D.B. Rawlins, J.T. Hunt, H. Xiao, S. Lu, L. Qian, W. Han, W. Shan, T. Mitt, Z. Cai, M.A. Poss, H. Zhu, J.S. Sack, J.S. Tokarski, C.Y. Chang, N. Pavletich, A. Kamath, W.G. Humphreys, P. Marathe, I. Bursuker, K.A. Kellar, U. Roongta, R. Batorsky, J.G. Mulheron, D. Bol, C.R. Fairchild, F.Y. Lee, K.R. Webster, Discovery of aminothiazole inhibitors of cyclin-dependent kinase 2: synthesis, X-ray crystallographic analysis, and biological activities, J. Med. Chem. 45 (2002) 3905–3927.
[20] S. Wang, C. Meades, G. Wood, A. Osnowski, S. Anderson, R. Yuill, M. Thomas, M. Mezna, W. Jackson, C. Midgley, G. Griffiths, I. Fleming, S. Green, I. McNae, S.-Y. Wu, C. Mclnnes, D. Zheleva, M. Walkinshaw, P.M. Fischer, 2-Anilino-4-(thiazol-5-yl)pyrimidine CDK Inhibitors: synthesis, SAR Analysis, X-ray crystallography, and biological activity, J. Med. Chem. 47 (2004) 1662–1675.
[21] C.J. Helal, M.A. Sanner, C.B. Cooper, T. Gant, M. Adam, J.C. Lucas, Z. Kang, S. Kupchinsky, M.K. Ahlijanian, B. Tate, F.S. Menniti, K. Kelly, M. Peterson, Discovery and SAR of 2-aminothiazole inhibitors of cyclin-dependent kinase 5/p25 as a potential treatment for Alzheimer's disease, Bioorg. Med. Chem. Lett. 14 (2004) 5521–5525.
[22] E. Schonbrunn, S. Betzi, R. Alam, M.P. Martin, A. Becker, H. Han, R. Francis, R. Chakrasali, S. Jakkaraj, A. Kazi, S.M. Sebti, C.L. Cubitt, A.W. Gebhard, L.A. Hazlehurst, J.S. Tash, G.I. Georg, Development of highly potent and selective diaminothiazole inhibitors of cyclin-dependent kinases, J. Med. Chem. 56 (2013) 3768–3782.
[23] T. Nasr, S. Bondock, M. Youns, Anticancer activity of new coumarin substituted hydrazide-hydrazone derivatives, Eur. J. Med. Chem. 76 (2014) 539–548.
[24] R. Pingew, A. Saekee, P. Mandi, C. Nantasenamat, S. Prachayasittikul, S. Ruchirawat, V. Prachayasittikul, Synthesis, biological evaluation and molecular docking of novel chalcone-coumarin hybrids as anticancer and antimalarial agents, Eur. J. Med. Chem. 85 (2014) 65–76.
[25] M.E. Riveiro, N. De Kimpe, A. Moglioni, R. Vazquez, F. Monczor, C. Shayo, C. Davio, Coumarins: old compounds with novel promising therapeutic perspectives, Curr. Med. Chem. 17 (2010) 1325–1338.
[26] M. Khoobi, S. Emami, G. Dehghan, A. Foroumadi, A. Ramazani, A. Shafiee, Synthesis and free radical scavenging activity of coumarin derivatives containing a 2-methylbenzothiazoline motif, Arch. Pharm. (Weinheim) 344 (2011) 588–594.
[27] X.-Q. Wu, C. Huang, Y.-M. Jia, B.-A. Song, J. Li, X.-X. Liu, Novel coumarin-dihydropyrazole thio-ethanone derivatives: design, synthesis and anticancer activity, Eur. J. Med. Chem. 74 (2014) 717–725.
[28] Y. Chen, H.-R. Liu, H.-S. Liu, M. Cheng, P. Xia, K. Qian, P.-C. Wu, C.-Y. Lai, Y. Xia, Z.-Y. Yang, S.L. Morris-Natschke, K.-H. Lee, Antitumor agents 292. Design, synthesis and pharmacological study of S- and O-substituted 7-mercapto- or hydroxy-coumarins and chromones as potent cytotoxic agents, Eur. J. Med. Chem. 49 (2012) 74–85.
[29] J.A. McKie, S.S. Bhagwat, H. Brady, M. Doubleday, L. Gayo, M. Hickman, R.K. Jalluri, S. Khammungkhune, A. Kois, D. Mortensen, N. Richard, J. Sapienza, G. Shevlin, B. Stein, M. Sutherland, Lead identification of a potent benzopyranone selective estrogen receptor modulator, Bioorg. Med. Chem. Lett. 14 (2004) 3407–3410.
[30] M. Nagarajan, A. Morrell, B.C. Fort, M.R. Meckley, S. Antony, G. Kohlhagen, Y. Pommier, M. Cushman, Synthesis and anticancer activity of simplified indenoisoquinoline topoisomerase I inhibitors lacking substituents on the aromatic rings, J. Med. Chem. 47 (2004) 5651–5661.
[31] A. Thakur, R. Singla, V. Jaitak, Coumarins as anticancer agents: A review on synthetic strategies, mechanism of action and SAR studies, Eur. J. Med. Chem. 101 (2015) 476–495.

[32] B.A. Christian, M.R. Grever, J.C. Byrd, T.S. Lin, Flavopiridol in the treatment of chroniclymphocytic leukemia, Curr. Opin. Oncol. 19 (2007) 573–578.
[33] a) D.H. Kim, H.K. Na, T.Y. Oh, C.Y. Shin, Y.J. Surh, Eupatilin inhibits proliferation of ras-transformed human breast epithelial (MCF-10A-ras) cells, J. Environ. Pathol. Toxicol Oncol. 24 (2005) 251–259;
b) N.A.A. Latif, R.Z. Batran, M.A. Khedr, M.M. Abdalla, 3-Substituted-4-hydroxycoumarin as a new scaffold with potent CDK inhibition and promising anticancer effect: synthesis, molecular modeling and QSAR studies, Bioorg. Chem. 67 (2016) 116–129.
[34] L.-Y. Li, J.-D. Peng, W. Zhou, H. Qiao, X. Deng, Z.-H. Li, J.-D. Li, Y.-D. Fu, S. Li, K. Sun, H.-M. Liu, W. Zhao, Potent hydrazone derivatives targeting esophageal cancer cells, Eur. J. Med. Chem. 148 (2018) 359–371.
[35] A. Jashari, F. Imeri, L. Ballazhi, A. Shabani, B. Mikhova, G. Dräger, E. Popovski, A. Huwiler, Synthesis and cellular characterization of novel isoxazolo- and thiazolohydrazinylidene-chroman-2,4-diones on cancer and non-cancer cell growth and death, Bioorg. Med. Chem. 22 (2014) 2655–2661.
[36] K.M. Amin, Y.M. Syam, M.M. Anwar, H.I. Ali, T.M. Abdelghani, A.M. Serry, Synthesis and molecular docking study of new benzofuran and furo[3,2-g]chromone-based cytotoxic agents against breast cancer and p38a MAP kinase inhibitors, Bioorg. Chem. 76 (2018) 487–500.
[37] J. Liu, F. Wu, L. Chen, L. Zhao, Z. Zhao, M. Wang, S. Lei, Biological evaluation of coumarin derivatives as mushroom tyrosinase inhibitors, Food Chem. 135 (2012) 2872–2878.
[38] K. Kasumbwe, K.N. Venugopala, V. Mohanlall, B. Odhav, Antimicrobial and antioxidant activities of substituted halogenated coumarins, J. Med. Plants Res. 8 (2014) 274–281.
[39] D. Chopra, K.N. Venugopal, B.S. Jayashree, T.N. Guru, Row, 3-acetyl-6-chloro-2H-chromen-2-one, Acta Crystallogr. E 62 (2006) 2310–2312.
[40] K.N. Venugopala, B.S. Jayashree, Mahesh Attimarad, Synthesis and evaluation of some substituted 2-arylaminocoumarinylthiazoles as potential NSAIDs, Asian J. Chem. 16 (2004) 872–876.
[41] F. Chimenti, A. Bolasco, D. Secci, P. Chimenti, A. Granese, S. Carradori, M. Yanez, F. Orallo, F. Ortuso, S. Alcaro, Investigations on the 2-thiazolylhydrazyne scaffold: Synthesis and molecular modeling of selective human monoamine oxidase inhibitors, Bioorg. Med. Chem. 18 (2010) 5715–5723.
[42] M.S. Refat, I.M. El-Deen, Z.M. Anwer, S. El-Ghol, Bivalent transition metal complexes of coumarin-3-ylthiosemicarbazone derivatives: Spectroscopic, antibacterial activity and thermogravimetric studies, J. Mol. Struct. 920 (2009) 149–162.
[43] J.A. Zoltewicz, L.W. Deady, Quaternization of heteroaromatic compounds: quantitative aspects, Adv. Heterocycl. Chem. 22 (1978) 71–121.
[44] Y.T. Kim, N.H. Cho, S.W. Park, J.W. Kim, Under expression of cyclin dependent kinase (CDK) inhibitors in cervical carcinoma, Gynecol. Oncol. 71 (1998) 38–45.
[45] H. Skomedal, G.B. Kristensen, A.K. Lie, R. Holm, Aberrant expression of the cell cycle associated proteins TP53, MDM2, p21, p27, cdk4, cyclin D1, RB, and EGFR in cervical carcinomas, Gynecol. Oncol. 73 (1999) 223–228.
[46] H. Okada, T.W. Mak, Pathways of apoptotic and non-apoptotic death in tumor cells, Nat. Rev. Cancer. 4 (2004) 592–603.
[47] Y. Kondo, T. Kanzawa, R. Sawaya, S. Kondo, The role of autophagy in cancer development and response to therapy, Nat. Rev. Cancer 5 (2005) 726–734.
[48] P.D. Mace, S.J. Ried, G.S. Salvesen, Chapter seven – caspase enzymology and activation mechanisms, Methods Enzymol. 544 (2014) 161–178.
[49] B.J. vanRaam, G.S. Salvesen, 3rd edition of Handbook of Proteolytic Enzymes, Enzymes 2 (2013) 2252–2255.
[50] G.S. Hassan, D.E. Abdel-Rahman, Y.S. Nissan, E.A. Abdelmajeed, T.A. Abdelghany, Novel pyrazolopyrimidines: synthesis, in vitro cytotoxic activity and mechanistic investigation, Eur. J. Med. Chem. 138 (2017) 565–576.
[51] K.M. Boatright, G.S. Salvesen, Mechanisms of caspase activation, Curr. Opin. Cell Biol. 15 (2003) 725–731.
[52] Rapid Miner 7.1.000 Basic Edition; Rapid Miner GmbH: Dortmund, Germany, 2016.
[53] I. Mierswa, M. Wurst, R. Klinkenberg, M. Scholz, T. Euler, YALE: rapid prototyping for complex data mining tasks, In: Proceedings of the 12th ACM SIGKDD international conference on Knowledge discovery and data mining; ACM: Philadelphia, PA, USA (2006) 935–940.
[54] O. Ritthoff, R. Klinkenberg, S. Fisher, I. Mierswa, S. Felske, YALE: Yet another learning environment. In LLWA'01 – Tagungsband der GI-Workshop-WocheLernen–Lehren – WissenAdaptivitat. University of Dortmund, Dortmund, Germany, Technical Report 763 (2001) 84–92.
[55] M. Shahlaei, Descriptor selection methods in quantitative structure–activity relationship studies: a review study, Chem. Rev. 113 (2013) 8093–8103.
[56] R.S. Pearlman, K.M. Smith, Novel software tools for chemical diversity, Persp. Drug. Disc. Des. 9 (1998) 339–353.
[57] G. Cruciani, P. Crivori, P.A. Carrupt, B. Testa, Molecular fields in quantitative structure–permeation relationships: the VolSurf approach, J. Mol. Struct (Theochem) 503 (2000) 17–30.
[58] P. Mahajan, G. Chashoo, M. Gupta, A. Kumar, P.P. Singh, A. Nargotra, Fusion of structure and ligand based methods for identification of novel CDK2 inhibitors, J. Chem. Inf. Model. 57 (2017) 1957–1969.
[59] A.M. Latham, J. Kankanala, G.W. Fearnley, M.C. Gage, M.T. Kearney, S. Homer-Vanniasinkam, S.B. Wheatcroft, C.W. Fishwick, S. Ponnambalam, In silico design and biological evaluation of a dual specificity kinase inhibitor targeting cell cycle progression and angiogenesis, PLoS One 9 (2014) e110997.
[60] A. Huwe, R. Mazitschek, A. Giannis, Small molecules as inhibitors of cyclin-dependent kinases, Angew. Chem. Int. Ed. 42 (19) (2003) 2122–2138.
[61] S.Z. Bin-bing, H. Zhang, M. Damelin, K.G. Geles, J.C. Grindley, P.B. Dirks, Tumour-initiating cells: challenges and opportunities for anticancer drug discovery, Nat. Rev. Drug Discov. 8 (2009) 806–823.
[62] K. Parang, G. Sun, Protein kinase inhibitors drug discovery, in: drug discovery handbook, John Wiley & Sons Inc, 2005, pp. 1191–1257.
[63] A.A. Russo, P.D. Jeffrey, A.K. Patten, J. Massagué, N.P. Pavletich, Structural basis of cyclin-dependent kinase activation by phosphorylation, Nature Struct. Biol. 3 (1996) 696–700.
[64] A. Daina, V. Zoete, A BOILED-Egg to predict gastrointestinal absorption and brain Penetration of small molecules, Chem. Med. Chem. 11 (2016) 1117–1121.
[65] F.J. Sharom, ABC multidrug transporters: structure, function and role in chemoresistance, Pharmacogenomics 9 (2008) 105–127.
[66] http://www.swissadme.ch/index.php.
[67] A. Daina, O. Michielin, V. Zoete, SwissADME: a free web tool to evaluate pharmacokinetics, drug-likeness and medicinal chemistry friendliness of small molecules, Sci. Rep. 7 (2017) 42717.
[68] C.A. Lipinski, F. Lombardo, B.W. Dominy, P.J. Feeney, Experimental and computational approaches to estimate solubility and permeability in drug discovery and development settings, Adv. Drug. Deliv. Rev. 46 (2001) 3–26.
[69] A.K. Ghose, V.N. Viswanadhan, J.J. Wendoloski, A knowledge-based approach in designing combinatorial or medicinal chemistry libraries for drug discovery. 1. A qualitative and quantitative characterization of known drug databases, J. Comb. Chem. 1 (1999) 55–68.
[70] D.F. Veber, S.R. Johnson, H.Y. Cheng, B.R. Smith, K.W. Ward, K.D. Kopple, Molecular properties that influence the oral bioavailability of drug candidates, J. Med. Chem. 45 (2002) 2615–2623.
[71] W.J. Egan, K.M. Merz, J.J. Baldwin, Prediction of drug absorption using multivariate statistics, J. Med. Chem. 43 (2000) 3867–3877.
[72] I. Muegge, S.L. Heald, D. Brittelli, Simple selection criteria for drug-like chemical matter, J. Med. Chem. 44 (2001) 1841–1846.
[73] T. Cheng, Y. Zhao, X. Li, F. Lin, Y. Xu, X. Li, Y. Zhang, R. Wang, L. Lai, Computation of octanol − water partition coefficients by guiding an additive model with knowledge, J. Chem. Inf. Model. 47 (2007) 2140–2148.
[74] J. Baell, M.A. Walter, Chemistry: chemical con artists foil drug discovery, Nature 513 (2014) 481–483.
[75] J.B. Baell, G.A. Holloway, New substructure filters for removal of pan assay interference compounds (PAINS) from screening libraries and for their exclusion in bioassays, J. Med. Chem. 53 (2010) 2719–2740.
[76] G. Thiessen, H. Thiessen, Microspectrophotometric cell analysis, Prog. Histochem. Cytochem. 9 (1977) 1–156.
[77] S. Diab, T. Teo, M. Kumarasiri, P. Li, M. Yu, F. Lam, S.K. Basnet, M.J. Sykes, H. Albrecht, R. Milne, S. Wang, Discovery of 5-(2-(phenylamino) pyrimidin-4-yl) thiazol-2(3H)-one derivatives as potent Mnk2 inhibitors: synthesis, SAR analysis and biological evaluation, Chem. Med. Chem. 9 (2014) 962–972.
[78] M. Andersson, J. Sjöstrand, A. Petersen, A.K.S. Honarvar, J.O. Karlsson, Caspase and proteasome activity during staurosporin-induced apoptosis in lens epithelial cells, Invest. Ophthalmol. Vis. Sci. 41 (2000) 2623–2632.
[79] http://www.rcsb.org/.
[80] A. Daina, O. Michielin, V. Zoete, iLOGP: a simple, robust, and efficient description of n-octanol/water partition coefficient for drug design using the GB/SA approach, J. Chem. Inf. Model. 54 (2014) 3284–3301.